Photometry and Imaging of the Coma With Narrowband Filters

David G. Schleicher

Lowell Observatory
1400 W. Mars Hill Road
Flagstaff, Arizona 86001

and

Tony L. Farnham

Dept. of Astronomy
University of Maryland
College Park, MD 20742

Review chapter accepted for publication in *Comets II*

The Lowell Observatory Preprint Series

Photometry and Imaging of the Coma with Narrowband Filters

David G. Schleicher
Lowell Observatory

Tony L. Farnham
University of Maryland

The use of narrowband filters to isolate light reflected by cometary grains and emitted by several gas species permits a wide variety of compositional and morphological studies to be performed. A brief survey of some of these studies is presented, along with detailed discussions of the techniques, procedures, and methodologies used. In particular, the advantages and disadvantages of both traditional photoelectric photometers and CCD cameras is explored, and an update is given regarding the new narrowband comet filter sets produced in recent years. Some of the unique aspects of narrowband filter reductions are characterized, as are the steps required in compositional studies. Finally, the most useful aspects of enhancing, measuring, and analyzing morphological features are investigated in detail.

1. INTRODUCTION AND BACKGROUND

In this chapter, we provide both a brief review and tutorial of the fields of narrowband photometry and narrowband imaging of comets. The use of narrowband filters to isolate the light emitted by various molecular species and reflected solar radiation by dust grains in cometary comae has a long and productive history, dating back nearly half a century (cf. *Schmidt and van Woerden*, 1957). While photoelectric photometers have been used throughout this interval, digital array detectors such as charge-coupled devices (CCDs) have now largely replaced photometers as the detectors of choice (cf. *Jewitt*, 1991). In spite of the overwhelming advantages CCDs provide in morphological studies, photometers continue to play an important role, particularly in chemical abundance studies.

Included here are discussions of the techniques, procedures, and methodologies used, and a survey of some of the physical and chemical properties that can be determined with these techniques, along with references to numerous examples. As such, in many respects this chapter is an update to the valuable review by *A'Hearn* (1983), where the issues of observational and reduction techniques were first summarized. We also include several topics in common with the more recent review by *Jewitt* (1991), in which his focus was on the types of studies obtainable with CCDs, but to minimize overlap, our emphasis is on the general topic of coma morphologies. As we have neither the space nor the desire to repeat details provided in previous summaries, we also urge the reader to examine several other excellent reviews in addition to those by A'Hearn and by Jewitt. In particular, a discussion of observations obtained in the early decades up to and including C/Kohoutek (1973 XII) are summarized by *Vanysek* (1976), while *Meisel and Morris* (1982) briefly review the topics of bulk brightness variations, narrowband and IR photometry, and early compositional studies. Photometry in the IR is also the focus of reviews by *Ney* (1982) and *Hanner and Tokunaga* (1991). Polarization studies are discussed by *Kolokolova et al.* (1997), *Levasseur-Regourd* (1999), and *Kolokolova et al.* (2004).

Some of the physical properties that can be determined for the coma include spatial profiles of individual gas species and of the dust, the presence or lack of jets, sporadic brightness variations or unusual coma morphology indicative of outbursts, periodic brightness variations or jet motions caused by nucleus rotation, and the color and polarization of dust grains. Analyses of many of these characteristics of the coma can yield strong constraints on nucleus properties, such as rotation period, pole orientation, and the number, location, and size of individual source regions on the surface of the nucleus. For some comets, in which the signal from the nucleus is not overwhelmed by that from the coma, one can also obtain direct measurements of the nucleus. Chemical composition studies that can be performed include the determination of relative abundances of different molecular species, and how these vary with heliocentric distance and/or orbital position and from comet to comet, and the absolute production rates of water and dust. With the application of an appropriate vaporization model, physical properties such as effective active areas and lower limits on the nucleus size can also be computed. Each of these topics is discussed in more detail either here or in other chapters (e.g., *Samarasinha et al.*, 2004; *Bockelée-Morvan et al.*, 2004; *Feldman et al.*, 2004; *Combi et al.*, 2004; *Fulle*, 2004).

2. INSTRUMENTATION

Although many early photometric studies, as well as many more recent imaging studies, have used wideband filters or even no filtration, in most cases the observer is inevitably left with an ensemble of reflected light from grains and emitted light from multiple gas species that cannot readily be disentangled. Exceptions to this generalization include nucleus studies at large heliocentric distances, where the coma is either nonexistent or sufficiently faint that the nucleus' signal can be extracted, and dust studies when an object is known to be gas-poor, or in the near-IR where gas emission is only a minor contaminant. To isolate individual emission bands or to obtain continuum measurements in the near-UV to near-IR region of the spectrum, one must either use narrowband filters or spectroscopic techniques, each of which has numerous strengths and weaknesses. Spectroscopic methods (cf. *Feldman et al.*, 2004, and references therein) have the advantage of permitting the observer to directly detect and measure the shape of spectral features, simplifying the task of separating emission lines and bands from the continuum. This is particularly important in the case of weak emission features, such as CH, NH_2, or [O I], where the contrast with respect to the local continuum is very low. However, even with a long-slit instrument or multiple apertures, only a very small fraction of the total coma is sampled at one time, and the signal-to-noise ratio (S/N) per spatial and per spectral resolution element drops rapidly as one samples farther from the nucleus and inner-coma. If sufficient time is available, mapping the coma can greatly improve the spatial coverage. In comparison, conventional photometry and imaging can sample a much greater portion of the coma at one time, but only for the stronger emission bands that can be reliably isolated with narrowband filters. And while both spectroscopy and imaging techniques permit investigations of gross asymmetries in the coma, such as sunward-tailward, only imaging readily permits more detailed morphological studies in the visible regime, such as those desired when studying dust and gas jets. However, the steady increase in the size of optical fiber bundles for two-dimensional spectroscopy implies that IFU spectroscopy may permit useful morphological studies in the future.

With the advent of the twenty-first century and improvements in digital detectors, one might expect that narrowband imaging would have completely superseded the technique of aperture photometry using conventional photoelectric photometers. While in principle this seems reasonable, in practice several issues have necessitated the continued use of conventional photometers for many types of compositional studies. The primary limitation of CCD detectors is the inherent level of noise at the per-pixel level due to readout noise and slight variations in bias level. While these sources of uncertainty are usually quite small (<1 count), they can still dominate over the cometary signal in many instances. As an example, it is quite common for the measured count level for OH or NH emission in a moderately bright comet (10th–12th magnitude) to be on the order of 100 counts per second within a relatively large photometric aperture of 1 arcmin. With a conventional photometer, this results in a photon statistical uncertainty of about 1% with less than 2 min of integration. With a CCD, however, the same ~10^4 photons are spread over ~10^4 pixels. Given the typical brightness fall-off away from the nucleus, a pixel 30 arcsec from the nucleus would, on average, only receive <0.2 photons during the equivalent exposure time — a value similar to or less than the inherent noise level associated with the read-out of each pixel. At such low signal levels, the absolute uncertainties associated with flatfielding also become quite important in determining the level of the background sky. It is hoped that the development of truly flat and readnoise-free CCDs will eventually mitigate these problems. Although aperture extractions from a CCD frame can be performed, obtaining images solely to extract aperture photometry of the coma largely defeats the advantages of a CCD, and the resulting photometric uncertainties are always worse than those associated with a simple photometer. Other practical concerns involve observing efficiencies, such as the effort required to obtain good twilight flatfield measurements for several narrowband filters, and the longer total time required to obtain sets of images of both the comet and sky in each filter, as compared to the time required with a photometer. As a result of all these issues, narrowband CCD observations have only rarely been calibrated and continuum subtracted to obtain gas column densities and abundances (cf. *Schulz et al.*, 1993).

For all these reasons, we have found that basic coma abundance measurements are much more readily obtained (and with much better S/N) using conventional photoelectric photometers. In our own work, we use a new, computer-controlled photometer, but with the same EMI 6256 S-11 phototube as used with our previous, manually operated photometer. This tube, with a quartz window, provides good throughput to wavelengths below the atmospheric cutoff in the UV and an extremely low dark current when thermoelectrically cooled, but has essentially no response in the red and near-IR. A variety of tubes, having a wide range of characteristics, remain available from several manufacturers. For details regarding construction and use of photoelectric photometers, we refer the reader to several books on this subject, particularly those by *Henden and Kaitchuck* (1982), *Sterken and Manfroid* (1992), and *Budding* (1993).

In contrast, CCD imaging is clearly the appropriate technique to employ if the primary goal is to study morphology or to extract the signal from the nucleus from that of the surrounding coma, rather than to obtain abundance measurements. In addition to advances in quantum efficiency, particularly in the UV, and readout noise suppression, perhaps the most important changes in CCD detectors in recent years for comet research have been the ever-increasing format sizes and the decreased overhead associated with readout times. Larger formats directly yield larger fractions of the coma being measured or may even extend to uncontaminated sky, while faster readout of the chip permits more filters to be used in a limited interval of time for both standard star measurements and twilight flats as well as for the

comet itself. Numerous books detailing the physical characteristics of CCD chips and/or observing and reduction techniques are now available, including those by *Jacoby* (1990), *Howell* (1992, 2000), and *Philip et al.* (1995).

3. NARROWBAND FILTERS

For both historical and practical reasons, the wavelength range within which narrowband filters have usually been constructed for comet studies has been between about 3000 and 7000 Å. The lower end of the range is set by the atmospheric cutoff, while the upper end is defined by the locations of the strongest emission bands for the observable species. For instance, although the CN molecule produces several emission bands between 7000 Å and 1.5 µm, each of these bands in the CN red system is much weaker than the primary band of the violet system at 3875 Å. Emission studies of comets in the UV (spacebased) and IR have nearly always been conducted using spectroscopic detectors, because the permanently installed filters are seldom useful for cometary studies (in the UV) or gas emission features are relatively weak. However, continuum studies in the IR have often made use of standard broadband filters such as J, H, and K.

A total of five neutral gas species produce sufficiently strong emission bands between about 3000 and 7000 Å to be easily isolated with narrowband filters. In order of wavelength, these are OH, NH, CN, C_3, and C_2. Figure 1 shows a composite spectrum, identifying the major emission features. Note that none of these species are assumed to exist in these forms in the nucleus, but each is instead at least a daughter species, produced by the dissociation of one or more parent (or grandparent) species. Appropriate modeling is therefore required to ultimately derive the nuclear abundances of the parents. Emission features by other neutral species, notably CH, NH_2, and O, are too weak and/or the species are too short-lived to remove the underlying continuum sufficiently accurately to produce reliable results in most circumstances. Emissions by two ion species, CO^+ and H_2O^+, have also been successfully isolated with narrowband filters. Unfortunately, as a consequence of the long wings of the C_3 and C_2 bands, together with the profusion of weak emission bands from NH_2 and other minor species, very few locations between 3000 and 7000 Å are completely absent of emission. This makes it difficult to obtain clean continuum measurements, and the decontamination of continuum measurements by gas emission is a significant issue to which we will return.

Over the past half-century, numerous investigators have had individual filters manufactured to isolate one or more of the stronger emission bands, often with accompanying continuum filters (cf. *Schmidt and van Woerden,* 1957; *O'Dell and Osterbrock,* 1962; *Blamont and Festou,* 1974; *A'Hearn and Cowan,* 1975). Unfortunately, the lack of standardization made it difficult to sort out the many discrepancies among the results. An initial effort at standardization was made in the late 1970s, when 3 sets of up to 10 filters were produced for use primarily at Lowell and Perth Observatories as the initial phase of the Lowell comet photometry program (cf. *A'Hearn et al.,* 1979; *A'Hearn and Millis,* 1980). A related effort at producing standard filter sets by an IAU Commission 15 Working Group resulted in design recommendations for a nine-filter set. Manufactured for worldwide distribution in time for Comet 1P/Halley's 1985/1986 apparition, several dozen sets were produced for photoelectric photometers and CCD cameras under the auspices of the International Halley Watch, and are now known as the IHW filters (cf. *Osborn et al.,* 1990; *A'Hearn,* 1991, *Larson et al.,* 1991). Representative transmission curves for the IHW filters are shown in Fig. 1.

Since the design of the IHW filters, several dust-poor comets have been observed spectroscopically, and the resulting spectra revealed that wings of the C_2 and, especially, the C_3 bands extended considerably further blueward than previously assumed, with the result that the IHW continuum filters at 3650 and 4845 Å suffered from much larger contamination than originally believed. In fact, for comets with very low dust-to-gas ratios, such as 2P/Encke, the wing of C_3 completely dominates the measured flux in the 3650-Å filter. It also became evident that the red continuum filter, centered at 6840 Å, was contaminated by an emission band tentatively identified as NH_2. Worse, as early as 1990 it was determined that some of the filters in some sets, including CN, were physically degrading, resulting in a decrease in the band transmission and a redward shift of the bandpass (cf. *Schleicher et al.,* 1991). This degradation of interference filters is unfortunately common, especially for bandpasses at wavelengths <4200 Å, because of older manufacturing techniques. By 1996, many observers had reported problems with their IHW sets, as they prepared to observe Comets Hale-Bopp (1995 O1) and Hyakutake (1996 B2). Because of the overwhelming interest in observing Hale-Bopp, NASA agreed to support the production of new sets of narrowband filters in time for Hale-Bopp's perihelion passage. In taking on the task of designing and calibrating these new sets, we decided to take advantage of improved manufacturing techniques, resulting in bandpasses being "squarer," i.e., having flatter tops and shorter wings, and filters with greater longevity and almost no variation of the bandpass with temperature. At the same time, we altered the placement of each of the continuum bandpasses to minimize the contaminations that were present in the IHW filters, and added an additional continuum point in order to better measure variations in dust reflectivity as a function of wavelength. The filter locations for the emission features were similar to those in the IHW sets, but with slight adjustments to take advantage of the squarer bandpasses and to minimize changes in the fractional transmission caused by the Swings effect, whereby the shape of the emission feature varies with heliocentric velocity and/or distance. Accommodations were also made for the shorter f-ratio systems that are increasingly used with CCD systems. A total of 48 full or partial sets of these 11 new filters were produced and distributed, and these have been designated the HB filter sets, since Hale-Bopp provided the motivation for their construction and was the initial target. The HB bandpasses are

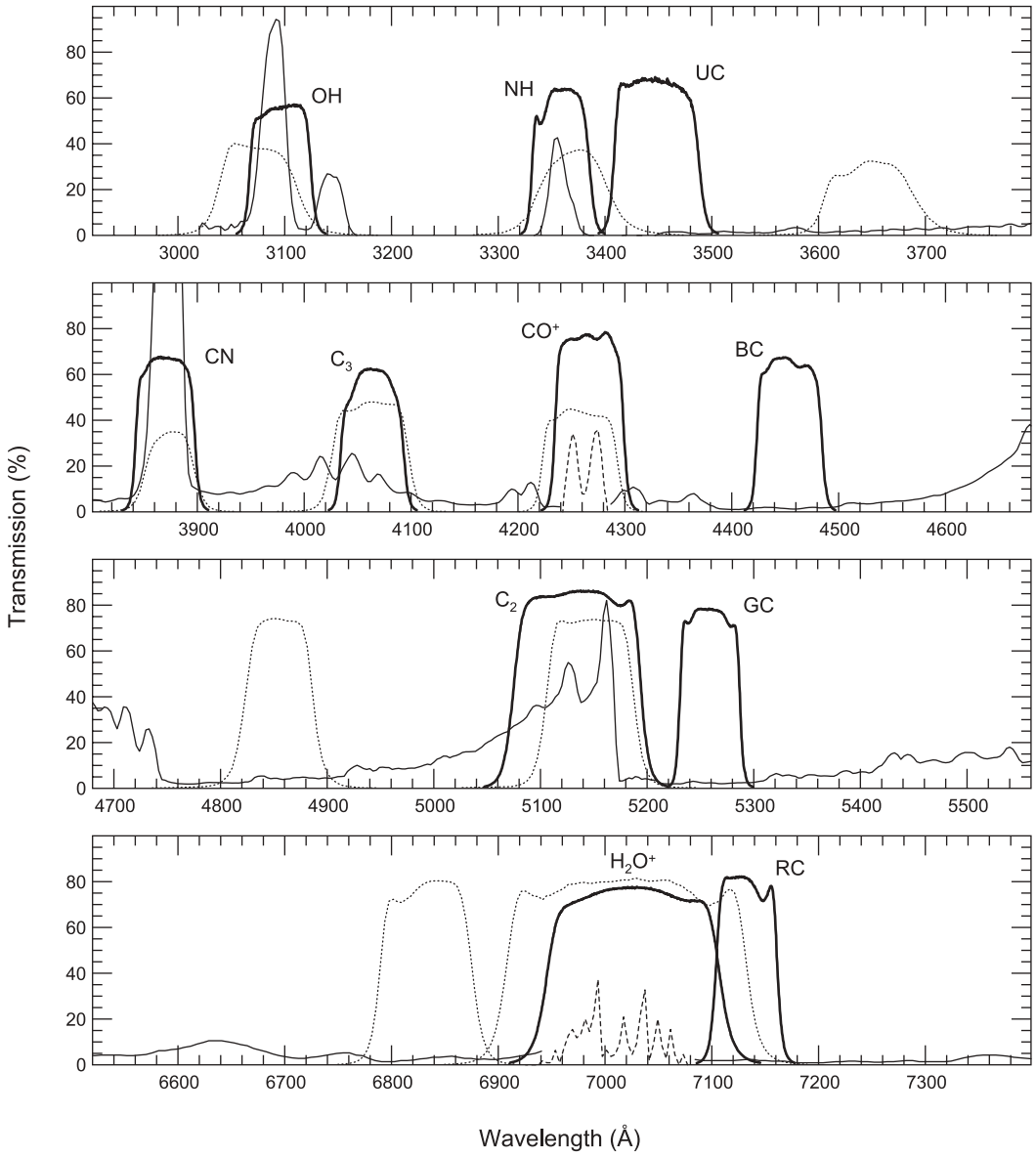

Fig. 1. Transmission profiles for the HB filters (thick lines) and IHW filters (dotted lines). For comparison, measured comet spectra illustrate the locations of the different emission bands. The neutral species and continuum regions are depicted by a spectrum of Comet 122P/deVico (spectral resolution = 12 Å) in the three top panels, and a spectrum of Comet 8P/Tuttle (resolution ~40 Å) in the bottom panel (thin solid lines). Because these comets do not exhibit clear ion bands, the 2–0 band of CO^+ from Comet 29P/Schwassmann-Wachmann 1 (resolution = 12 Å) has been inserted from 4240 to 4265 Å in the second panel and the 0–6–0 band of H_2O^+ from Comet Kohoutek 1973 E1 (resolution = 5 Å) has been inserted from 6940 to 7080 Å in the bottom panel (dashed lines). The 122P/deVico spectrum is courtesy of A. Cochran, and the 8P/Tuttle spectrum, created by S. Larson and J. Johnson, is courtesy of S. Larson. The CO^+ band was extracted from *Cochran and Cochran* (1991) and *Cochran et al.* (1991), and the H_2O^+ band was extracted from *Wehinger et al.* (1974) and *Wyckoff and Wehinger* (1976). From *Farnham et al.* (2000).

presented in Fig. 1 and itemized in Table 1; details of the individual filter design criteria and associated issues are available in *Farnham et al.* (2000).

Shortly prior to our efforts to design and produce the HB filter sets, ESA began a similar effort to produce new filters to replace the aging IHW sets. In ESA's case, the primary motivation was to observe the *Rosetta* spacecraft target, Comet 46P/Wirtanen, during its 1996/1997 and future apparitions. Due to a variety of issues, including the timing of the availability of funding and requirements regarding the choice of manufacturers, the ESA and NASA efforts proceeded mostly independent of one another, with somewhat different design preferences and specifications. A total of 18 sets of these ESA filters for support of the *Rosetta* mission were produced and distributed. These bandpasses are also listed in Table 1. Because most of the HB and ESA

TABLE 1. Characteristics of new narrowband comet filters.

	Bandpass† (Å)	
Species*	HB Sets	ESA Sets
OH (0–0)	3090/62	3085/75
NH (0–0)	3362/58	—
UV Continuum	3448/84	—
CN ($\Delta v = 0$)	3870/62	3870/50
C_3 (Swings System)	4062/62	4060/70
CO^+ (2–0)	4266/64	—
Blue Continuum	4450/67	4430/40
C_2 ($\Delta v = 0$)	5141/118	5125/125
Green Continuum	5260/56	—
NH_2 (0,2,0)	—	6630/60
H_2O^+ (0,6,0)	7020/170	—
Red Continuum	7128/58	6840/90

*Emission band designations in parentheses.
†Nominal center wavelength and full-width half-maximum (FWHM).

filter sets were intended for use with CCD cameras, several differently sized filters were produced, ranging from 25 to 100 mm and 25 to 80 mm respectively.

A wide variety of issues must be addressed when calibrating a filter set, including the selection and calibration of standard stars, the determination of reduction coefficients for the calculation of absolute fluxes, and, specifically for comet filters, the determination of nonlinear extinction coefficients for the reduction of the OH band measurements, and coefficients for the decontamination of continuum filters and the removal of continuum from the emission bands. These are discussed in some detail by *A'Hearn* (1983) and references therein, and, for the IHW filter sets, in *Osborn et al.* (1990) and *A'Hearn* (1991). Because a complete discussion of these issues as applied to the new HB filter sets is contained in *Farnham et al.* (2000), we next provide only an abbreviated summary; we use the HB filters as an example, since the calibration of the ESA filter sets is currently in progress.

The usefulness of a new filter set is entirely dependent on the availability of suitable standard stars. In the case of comet observations, two types of standards are needed: flux standards, used to determine atmospheric extinction and to convert relative magnitudes to absolute fluxes, and solar analogs, used to mimic the solar spectrum in determining the spectral reflectivity of the dust or nucleus and for continuum subtraction from the emission bands. For these latter objectives, the key issue is selecting stars that best match the color of the Sun. Since no star has yet been identified as a true "twin" of the Sun, and there are differences among researchers as to which star most closely matches the Sun, we measured a dozen known solar analogs using the HB filters and discovered a surprisingly large dispersion in colors in the near-UV. Because several of these stars are considered close solar analogs, we removed three other stars whose colors were most discrepant. We also wanted to evenly bracket the Sun's physical properties, such as temperature, metallicity, and chromospheric activity, resulting in the removal of two additional stars that skewed the brackets. Ultimately, colors of seven solar analogs — HD 25680, 18 Sco, 16 Cyg A, vB 106, 16 Cyg B, vB 64, and HD 76151 (in order of their colors in the near-UV) — were averaged and adopted as representative solar colors, and these have been incorporated in the various reduction coefficients. Therefore, if an investigator uses the equations and coefficients listed in *Farnham et al.* (2000), solar analogs do not need to be included in the observing program.

Unlike solar analogs, flux standards must be observed nightly, to determine both the amount of atmospheric extinction and the instrumental corrections associated with each filter. For the HB filters, a total of 24 stars were selected having spectral types of late-O to late-B and V magnitudes ranging from 4th to 8th. Besides the obvious need to be nonvariables, relatively hot stars are preferred to minimize the number of spectral absorption features and to maximize the flux in the UV. The stars are nearly uniformly distributed near the celestial equator, insuring that some stars would match the airmass of any comet within 1–2 h of the comet observations. The brighter flux standards provide excellent S/N for photometric systems on smaller telescopes, while the fainter stars are suitable for many CCD systems by minimizing the need to defocus the image to prevent saturation.

4. DATA ACQUISITION AND REDUCTION

Basic data acquisition and reduction of a night's observations follow conventional procedures except for a few notable exceptions unique to cometary data. The first exception is that observations must often be obtained at high air mass due to a comet's proximity to the Sun. This fact, coupled with the number of species that have their primary emission bands in the near-UV, implies that precise extinction coefficients must be determined on a nightly basis, requiring standard star measurements over a range of airmasses bracketing the airmass range of the comet. Fortunately, because the filters have relatively narrow bandpasses, no color terms are required in the reductions, except for the OH filter near 3100 Å. In this unique case, extinction varies significantly across the bandpass, due to the strong wavelength-dependence of the ozone component of extinction. Moreover, the resulting curvature of the extinction-airmass relation differs with the detailed spectral signature being measured, and therefore different reduction coefficients are required for flux standards and for comets having differing gas-to-dust ratios. The appropriate equations and coefficients for extinction with the HB OH filter are detailed in *Farnham et al.* (2000).

The need to accurately remove contamination by emission bands of the continuum filters in high gas-to-dust ratio comets, and to subtract continuum from emission bands in low gas-to-dust ratio comets, requires sufficiently high S/N for whichever filters yield the smallest count levels. This implies that the optimum integration times for each filter will not only differ due to the overall brightness of the comet, but also with the relative amounts of gas and dust. It is therefore highly desirable to reduce the first observations of a new comet rapidly so as to be able to tailor

subsequent observations. Accurate determinations of the background sky with each filter are also necessary, and can be very time-consuming to obtain. Typically, if a comet is sufficiently bright to enable the use of narrowband filters, the coma is likely to cover the entire CCD frame, forcing one to obtain separate sky frames for each filter. It is generally sufficient to obtain sky measurements at distances greater than ~30 arcmin from the nucleus in any direction other than that of the tail, although larger distances are required for exceptionally bright or close comets. It is also almost always preferable to track at the comet's rate of motion across the sky when obtaining either photometry or imaging of the coma; this capability is more routine now that most telescopes are computer-controlled.

When performing small-aperture extractions from CCD images, one must be aware of the effects of changing amounts of flux from the coma and from the nucleus due to seeing variations during the night; otherwise, artificially produced lightcurve features can result. While these effects can be searched for by extracting fluxes from a series of apertures, compensating for this situation is extremely difficult unless the effective pointspread function is available on each frame, and background stars will be trailed unless the exposures are kept sufficiently short. Decisions regarding appropriate aperture sizes for a conventional photometer must be made at the time the observations are acquired. Here, some major tradeoffs must be made to (1) avoid background stars, (2) minimize the sky signal, and (3) maximize the comet signal. With either instrumentation, practical limitations on integration times are imposed by (1) changing sky brightness (particularly near twilight), (2) total time the comet is available, and (3) the number of filters to be used. Compromises must almost always be made; the observer should let the specific science goals determine the best observing procedures on a case-by-case basis.

Except for the nonlinear extinction associated with the OH filter and already discussed, reductions to filter fluxes follow standard methods. Thereafter, narrowband reductions are somewhat unusual, in that the continuum filters often suffer from some contamination from cometary emission bands, the emission filters include underlying continuum, and the continuum is often reddened with respect to solar spectrum. A new iterative technique was developed by *Farnham et al.* (2000) to deal with these issues when using the HB filters. This procedure uses the measured fluxes in the continuum bands to remove underlying continuum from the C_3 and C_2 filter fluxes, which can then be used to compute the amount of contaminating emission in the continuum filters. At each step of the iteration the remaining contamination is reduced, until essentially pure emission fluxes and continuum fluxes are obtained. Again, all relevant equations and coefficients are provided in *Farnham et al.* (2000).

5. COMPOSITIONAL PHOTOMETRY

As previously noted, comet photometry for the purposes of compositional determinations can be made using either a phototube or a CCD as a detector, but the former usually results in improved S/N for a given amount of observing time. This section is therefore primarily aimed at, but not restricted to, observations obtained with a conventional photometer system. Of course, many of the following procedures have direct analogs in the analysis of comet spectrophotometry.

The derived continuum fluxes and emission band fluxes are usually the final reduced quantities that can be considered model-independent. In the typical case of comets with detectable coma, unlike for point sources, the aperture used for the measurements must be specified for these quantities to be meaningful. Usually the observer will also want to compute an aperture-independent quantity by applying a suitable model of the coma, after first converting gas emission band fluxes to the number of molecules required to produce the measured fluxes. This conversion to a molecular abundance requires the use of the fluorescence efficiency (L/N or luminosity per molecule when given in units of ergs per second per molecule, or, equivalently, g-factor when given in units of photons per second per molecule) for the particular molecular band. While the fluorescence efficiencies for comets are generally unchanging for polyatomic species due to their large number of populated rotational levels (except for the r^{-2} dependence due to the fall-off of solar flux with distance from the Sun), diatomic molecules such as OH, NH, and CN display large variations as a function of heliocentric velocity due to the Swings effect (cf. *Arpigny*, 1976; *Feldman et al.*, 2004). Appropriate values as a function of velocity for OH can be found in *Schleicher and A'Hearn* (1988), for NH in *Kim et al.* (1989) and *Meier et al.* (1998), and for CN in *Tatum and Gillespie* (1977), *Schleicher* (1983), and *Zucconi and Festou* (1985). Note that the latter two CN references also present the variation of the fluorescence efficiencies as a function of heliocentric distance as well as with velocity, since the number of populated rotational levels in CN varies strongly with the available solar flux. In the Lowell photometric program, we currently continue to use the same fluorescence efficiencies adopted by *A'Hearn et al.* (1995), and these are summarized in Table 2. However, the values for some species, such as C_3, may change in the future as band oscillator strengths are revised or as fluorescence models include more transitions and collisional effects.

The resulting molecular abundances obtained following the application of fluorescence efficiencies can be readily converted to column densities, if desired, but for either abundances or column densities the size and location of the aperture or slit must be stated for the result to be useful. In order to intercompare results obtained with differing apertures on a single comet or to intercompare comets, a coma model (such as the Haser, the Vectorial, or a numerical model such as the Monte Carlo) is applied to extrapolate the measured column abundance to a total coma abundance. While there are pros and cons to each specific model (see *Combi et al.*, 2004, and references therein), in each case a few parameters (such as the lifetime, velocity, and/or scale-length) are used to approximate the spatial distribution of the specific gas species in cometary comae. Once a total coma

TABLE 2. Adopted parameters used in reduction of Lowell narrowband photometry.

Species	L/N* (erg s^{-1} mol^{-1})	Reference	Haser Scalelength† Parent (km)	Haser Scalelength† Daughter (km)	Daughter Lifetime† (s)	Reference
OH (0–0)	1.4–8.3 × 10^{-15}	*Schleicher and A'Hearn* (1988)	2.4 × 10^4	1.6 × 10^5	1.6 × 10^5	*Cochran and Schleicher* (1993)
NH (0–0)	4.9–7.6 × 10^{-14}	*Kim et al.* (1989)	5.0 × 10^4	1.5 × 10^5	1.5 × 10^5	*Randall et al.* (1992)
CN (Δv = 0)	2.4–5.0 × 10^{-13}	*Schleicher* (1983)	1.3 × 10^4	2.1 × 10^5	2.1 × 10^5	*Randall et al.* (1992)
C_3 (λ4050)	1.0 × 10^{-12}	*A'Hearn et al.* (1985)	2.8 × 10^3	2.7 × 10^4	2.7 × 10^4	*Randall et al.* (1992)
C_2 (Δv = 0)	4.5 × 10^{-13}	*A'Hearn* (1982)	2.2 × 10^4	6.6 × 10^4	6.6 × 10^4	*Randall et al.* (1992)

*All fluorescence efficiencies (L/N; for r_H = 1 AU) are scaled by r_H^2. L/N for OH, NH, and CN are functions of $\dot{r}_H$, and L/N for CN is also a function of r_H (see *A'Hearn et al.*, 1995, for details). The CN (0–0) L/N values are multiplied by 1.08 to approximate the contribution of the CN (1–1) band.
†All scale lengths and lifetimes (for r_H = 1 AU) are scaled by r_H^{-2} (see *A'Hearn et al.*, 1995, for details).

abundance is computed, this quantity can be divided by the lifetime of the species (usually controlled by the photodissociation rate from solar radiation) to compute the production rate of the species, Q, i.e., the rate at which new molecules (or their parents) must be released from the nucleus to maintain the observed abundance. Unfortunately, the values for these seemingly fundamental parameters are often poorly known, because many of the species are radicals and therefore difficult to measure in the laboratory. Moreover, lifetimes also vary with solar activity, while the amount of acceleration of the bulk gas flow varies with collision rates, which depend upon the total gas production rate and the distance from the nucleus.

To minimize the number of parameters needed when intercomparing the composition of comets, the Lowell program generally uses the Haser model, again with the same values for the model parameters as those adopted by *A'Hearn et al.* (1995), and these are also summarized in Table 2, along with assumed daughter lifetimes. These particular values were based on observed radial profiles obtained over a variety of heliocentric distances, but they do not work in all circumstances. For instance, in the case of Comet Hale-Bopp, the scalelengths must be increased by 2–3× due to the combination of unusually large gas outflow velocities in this very high production comet along with low solar activity (*Schleicher et al.*, 1999). For these and other reasons, to the extent possible it is important to observationally verify the validity of the parameters used in this modeling, such as by directly measuring the radial profiles of each gas species, either by observing with multiple photometer entrance apertures, narrowband imaging, or longslit spectroscopy. Unfortunately, in practice, this testing of the parameters is usually not feasible except with relatively bright comets.

A method to produce an aperture-independent quantity utilizing continuum flux measurements of the dust coma was introduced by *A'Hearn et al.* (1984). This quantity, $A(\theta)f\rho$, is the product of the bond albedo, A, at a particular phase angle, θ, the filling factor, f, and the projected aperture radius, ρ, as seen on the sky plane. This product will be independent of aperture size if the dust follows a canonical $1/\rho$ spatial distribution for outflowing dust, and will be independent of wavelength if the dust has no color as compared to the Sun. The equation to compute $A(\theta)f\rho$, as well as the appropriate values for the conversion coefficient for each HB continuum filter, are given in Appendix D of *Farnham et al.* (2000). Since no knowledge of the grain properties is required as input to the calculation, the computation of $A(\theta)f\rho$ from the measured continuum flux is straightforward, and therefore $A(\theta)f\rho$ is often used as a proxy of dust production, somewhat analogous to the gas production rates discussed above. Indeed, the quantity $A(\theta)f\rho$ varies proportionally to the dust release rate from the nucleus, but also inversely proportional to the dust outflow velocity. Unfortunately, the very fact that grain properties are not included in $A(\theta)f\rho$ means that intercomparisons as a function of time for a single comet or intercomparisons between comets must be made with caution. Simple intercomparisons inherently assume that numerous properties of the dust grains are constant with time and among comets, such as particle size distribution, grain shape and porosity, and outflow velocity. However, since dust grains are initially entrained with the gas flow, the resulting bulk dust velocity can vary with total gas production rates. Particle size distributions are known to differ drastically among comets, and outflow velocities also vary with particle size. Grains have also been seen to "fade" as they move away from the nucleus, either by shrinking in size or darkening as volatiles escape from the grains, or by breaking apart (*Jewitt and Meech*, 1987; *Baum et al.*, 1992). Therefore, it can be difficult to determine whether a particular variation or trend of $A(\theta)f\rho$ is actually a measure of the rate of release of dust grains from the nucleus, or an indication of differing grain properties, as was determined in the recent case of Comet 19P/Borrelly (*Schleicher et al.*, 2003).

A variety of types of scientific studies that can be performed from photometric measurements obtained through narrowband filters was itemized in the introduction to this chapter. We now briefly explore a selected subset of these topics, primarily drawing on examples from our own work simply because, following the apparition of Comet 1P/Halley in 1985/1986, very few groups have continued to employ this technique. Certainly one of the most basic types of studies are those of relative gas and dust production rates to determine the relative composition of parent or grandparent species in the nucleus (or, at least, the active source regions on the nucleus). Differences in the abundance ratios as a comet moves along its orbit can be used to infer

chemical inhomogeneities in the nucleus (e.g., *A'Hearn et al.,* 1985), while differences among comets can indicate either evolutionary effects, such as the strong gas-to-dust variation with perihelion distance (*A'Hearn et al.,* 1995), or primordial, such as the large fraction of Jupiter-family comets that are depleted in carbon-chain molecules as shown in Fig. 2 (*A'Hearn et al.,* 1995). With a sufficiently large database, such as the 85 comets observed by *A'Hearn et al.* (1995), numerous compositional investigations were possible on a statistical basis. Of course, other properties, such as heliocentric distance-dependencies and possible variations with species, can be determined for well-studied comets such as 1P/Halley (*Schleicher et al.,* 1998a), 2P/Encke (*A'Hearn et al.,* 1985), 21P/Giacobini-Zinner (*Schleicher et al.,* 1987), and Hyakutake (1996 B2) (*Schleicher and Osip,* 2002). By utilizing a basic water vaporization model (cf. *Cowan and A'Hearn,* 1979), minimum effective active areas on the surface of the nucleus can be computed, yielding a minimum effective radius or, if the nucleus size is determined separately, a fractional active area. One of the most unexpected results from the Lowell photometry program is the large number of comets having very small (<3%) active fractions (*A'Hearn et al.,* 1995).

The color of dust grains is primarily an indicator of the particle size(s), and has limited value in determining other physical properties of the grains, such as composition or porosity (cf. *Kolokolova et al.,* 2004). Measurements of phase effects, particularly at small and large phase angles, are difficult to obtain because of other, often stronger sources of brightness variations, such as a comet's changing heliocentric distance. A few comets for which phase effects have been successfully separated from other effects include P/Stephan-Oterma (*Millis et al.,* 1982), Bowell (1980b) (*A'Hearn et al.,* 1984), and Halley (*Meech and Jewitt,* 1987; *Schleicher et al.,* 1998a). The most diagnostic type of remote measurements for dust particles in cometary comae is that of polarization. These can usefully constrain physical properties, but are difficult to obtain. Here, again, narrowband filters minimize the contamination otherwise caused by gas emission. One research group that has routinely obtained this type of narrowband measurements is that of Kiselev and Chernova and their associates (cf. *Kiselev and Chernova,* 1981; *Chernova et al.,* 1993; *Kolokolova et al.,* 2004). Note that narrowband filters have also been occasionally used to obtain polarimetric measurements of molecular gas emission (cf. *Le Borgne et al.,* 1987; *Sen et al.,* 1989), but the degree of polarization is generally much smaller for gas than for dust and underlying continuum must be very accurately removed, making gas polarization measurements quite difficult.

Finally, periodic variations detected within a photometric lightcurve can, of course, be used to determine the rotation period of a comet nucleus. While variations due to the changing cross-section of the nucleus itself are most easily interpreted (and are most readily obtained using a CCD), measured variations of the brightness of the coma can be used to infer the number and relative strengths of individual source regions on the surface of the nucleus. Differences in lightcurve amplitudes and phase lags among the various gas species and with the dust can further be used to constrain outflow velocities and lifetimes, as in the cases of Comets 1P/Halley (cf. *Millis and Schleicher,* 1986), Levy (1990c) (*Schleicher et al.,* 1991), and Hyakutake (1996 B2) (*Schleicher and Osip,* 2002).

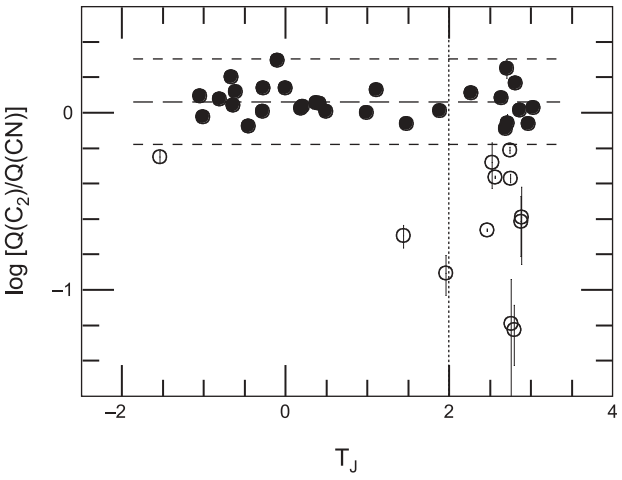

Fig. 2. Derived production rate ratios of C_2 to CN as a function of the Tisserand invariant with respect to Jupiter, T_J. The C_2-to-CN ratios are based on each species' respective ratio to OH. Comets having "typical" composition are those within the horizontal band (●), while carbon-chain depleted comets lie below this band (○). One-half of Jupiter-family comets ($T_J > 2$) are depleted, while only two non-Jupiter-family comets ($T_J < 2$) display significant depletions, and one of these — P/IRAS — oscillates across the $T_J = 2$ boundary. Statistically, most Jupiter-family comets are believed to have originated in the Kuiper belt, while most other comets should have come from the Oort cloud. Based on *A'Hearn et al.* (1995).

6. IMAGING AND COMA MORPHOLOGY

6.1. Morphological Features

Many comets exhibit detailed, well-defined features in their comae. The presence of these features indicates that the surfaces of the nuclei of these comets are not uniformly active, but emit material anisotropically, with at least part of the material coming from isolated active areas. Some of the more prominent types of features that are observed include jets (radial structures produced by isolated active regions, or sources, that emit collimated streams of gas and dust), fans (jet-like structures that tend to be broader and more diffuse than jets), spirals and arcs (outflowing material from jets on a rotating nucleus that form archimedean spirals, or partial segments of spirals, respectively), and coma asymmetries (some regions of the coma appear brighter than others). In addition to providing an explanation for the coma morphology, the existence of isolated source regions also provides a natural explanation for a variety of other phenomena observed in comets, including seasonal variations in the production rates, nongravitational accelerations of the

comet's orbit, and changes in the rotation state of the nucleus. Because isolated source regions can contribute to so many different aspects of the comet's activity, it is important to determine their characteristics.

To fully understand the role that the active regions play in the comet's behavior, properties such as the rotation state of the nucleus and the location of the sources must also be known, so that the dust and gas emission can be characterized as a function of time. Frequently, models of jet emissions can be used to reproduce the observed morphology and infer the relevant properties of the nucleus. Furthermore, in certain situations, it is possible to utilize these derived results to aid other analyses. Potential secondary studies include searching for compositional inhomogeneities in the jets (cf. *A'Hearn et al.,* 1986a,b; *Lederer et al.,* 1997; *Festou and Barale,* 2000) or constraining more fundamental characteristics such as the mass and density of the nucleus (*Farnham and Cochran,* 2002). Although some of the properties determined through coma modeling could be found using other techniques (e.g., lightcurve variations may reveal the rotation period), many could otherwise only be found via spacecraft encounters. This makes the analysis of the coma morphology an extremely valuable technique for understanding the fundamental qualities of cometary nuclei.

The majority of studies involving analysis of a comet's coma features are performed using images obtained with broadband or continuum filters. This is likely due to two factors: The dust coma tends to show clearer, more well-defined structures than the gas species, and the data reduction process is simpler. However, while they have proven to be very useful, dust images only provide a partial picture of the overall coma morphology, with gas and ions adding their own contributions. In most comets, features in the gas coma tend to be completely overwhelmed by the dust, but narrowband filters can be used to help isolate the gas features. Then, as described previously, with careful calibration the underlying continuum can be removed, leaving images of the pure gas coma (*Schulz et al.,* 1993, 2000; *Farnham et al.,* 2000). (Similarly, gas contamination can be removed from images obtained with narrowband continuum filters to leave the pure dust coma.) The pure gas images can then be enhanced or modeled, in the same manner as the dust images, to learn about the gas properties and to provide additional constraints on the nucleus properties. Studies of the CN coma in Comet Hale-Bopp illustrate the potential benefits of utilizing the gas morphology: First, the CN forms complete spirals around the nucleus, while only partial arcs are seen in the continuum (see Fig. 3), indicating that the gas production behaves differently from that of the dust (*Larson et al.,* 1997; *Farnham et al.,* 1998b; *Mueller et al.,* 1999). Second, the CN spirals expand radially outward at about twice the speed of the dust features, which is likely due to differences in initial outflow velocities and accelerations (*Schleicher et al.,* 1999). The fact that the gas and dust are not co-spatial indicates that most of the gas is being emitted directly from the nucleus rather than coming from the optically important dust grains in the coma. Third, the CN images clearly show three distinct jets in each rotational cycle, while the dust shows only two, which might suggest inhomogeneities in the nucleus. Finally, *Woodney et al.* (2002) used narrowband filter data, in conjunction with radio measurements of the spatial structure, to explore the relationship between the HCN and CN.

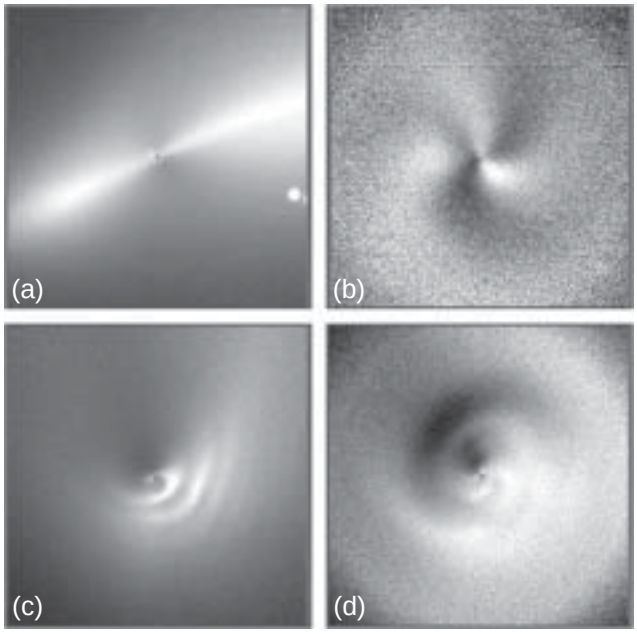

Fig. 3. Comparison of radial and azimuthal features, and the differences between dust and gas morphology. **(a)** Comet Borrelly showing purely radial structure (*Farnham and Cochran,* 2002). **(b)** CN jets observed in Comet Halley, showing initially radial features with curvature induced by rotation of the nucleus (*A'Hearn et al.,* 1986a; *International Halley Watch,* 1995). **(c)** Dust and **(d)** CN images of Comet Hale-Bopp, showing azimuthal features and the difference between the structure of the gas and dust in the coma (*Farnham et al.,* 1999). Features were enhanced by dividing out a $1/\rho$ profile from the dust frames and an azimuthal-averaged profile from the CN images.

Investigations of the nucleus size and the cometary plasma environment can both benefit from the use of narrowband filters, too. For high gas-to-dust comets, direct measurements of the nucleus (*Lamy et al.,* 2004) are more efficient with narrowband filters than broadband ones, because continuum filters exclude the gas contribution and make the nucleus stand out more against the coma. In plasma tail studies, the narrow passbands will isolate CO^+ or H_2O^+ much more efficiently than broadband filters or photographic plates, increasing the contrast of the plasma features against the background. Furthermore, with proper calibration, the continuum can be removed from the ion images to reveal the features very close to the nucleus. This improves the potential for following phenomena such as disconnection events from their earliest stages (*Ip,* 2004).

Dust, gas, and ion features have been observed and studied in many comets, with recent examples including Halley, Hyakutake, Hale-Bopp, and Borrelly. Although the detailed morphology in each comet is unique, the features can generally be classified into two main categories: azimuthal and

radial (or a combination of the two). Because most of the material from a jet expands radially away from the surface, the appearance of structures in the coma is strongly dependent on the geometric viewing conditions and the rotation state of the nucleus. A source at a given latitude will sweep out a hollow cone centered on the spin axis (or a partial cone if the source rotates out of sunlight and shuts down during part of a rotation). When Earth is oriented inside the cone, features usually appear to be azimuthal — archimedean spirals when the source is continuously illuminated and concentric arcs when it turns on and off. If Earth is outside the cone, then the feature may appear to oscillate back and forth, or it may smear together to produce a fan with primarily radial structures [due either to the planetary nebula effect at the edges of the fan or to insufficient spatial resolution (*Samarasinha et al.*, 1999)]. Radial features are also produced when the jet is on a slowly rotating nucleus (e.g., seeing only the innermost segment of the archimedean spiral, which is nearly radial) or if the active region is near the rotation pole, as is the case for Comet 19P/Borrelly (*Samarasinha and Mueller,* 2002; *Farnham and Cochran,* 2002; *Schleicher et al.*, 2003).

We note that factors other than isolated active regions can also produce features in the coma. Solar radiation pressure can act on the dust grains to produce envelopes that can be mistaken for arcs, while anti-tails and neck-line structures can mimic radial structures (*Fulle,* 2004). However, both of these cases are only observed in continuum images and involve relatively unique circumstances and geometric alignments, which can be investigated to avoid misinterpretation of the results. Structure in the coma can also result from outflowing material that experiences constructive interference and density enhancements due to the topology of the nucleus (*Crifo et al.*, 2004), but this mechanism can only produce features that are restricted to the very innermost coma regions and have a low contrast against the background. Finally, other types of features, such as knots, condensations, and kinks, are observed in plasma tails, but these are not addressed in any detail here.

6.2. Image Enhancement Techniques

Any comprehensive discussion of the coma morphology, gas, dust, or plasma, must inevitably address the topic of image enhancement techniques, as the two are intimately related. Indeed, many features are overwhelmed by the bulk radial brightness fall-off of the coma and only become obvious when the image has been processed in some manner (though once the user knows what to look for, the features are usually detectable in the unenhanced image with appropriate display parameters). Unfortunately, enhancing an image, by definition, alters the image, and not always in the manner that is expected or desired. Thus, any processing technique should be used with caution. Potential dangers include introducing artifacts that can be misinterpreted as real structures or shifting the apparent positions of features. Even if these shifts are small (which is not always the case), they are misleading when they change the positions that are being used to constrain models of the morphology. Another potential problem with enhancing an image is that various techniques may reveal different types of features in a given image. Because of this, the interpretation of the nature of the feature may be strongly dependent on the particular technique as well as on the manner in which it was applied. For example, images of Comet Hyakutake processed with a $1/\rho$ removal (discussed below) appear to have round blobs of material moving radially outward, while processing with radial profiles derived from the comet itself reveal that the blobs are actually broad spiral arcs (cf. Figs. 4b and 4k) (*Schleicher et al.*, 1998b; *Schleicher and Woodney,* 2003). Finally, enhancement of an image inherently changes the relative intensities of the different regions of the coma. This is a concern in the interpretation of the relative brightnesses and strengths of the different sources, as well as in using coma asymmetries to constrain the gas and dust production as a function of solar illumination.

There are a wide variety of enhancement techniques, each of which has its own strengths and drawbacks. Any technique can be good or bad and no single technique is ideal for every situation. Thus, it is important for the user to experiment with different methods on a variety of data, to become familiar with their pros and cons, to understand the types of data for which specific techniques are most useful, and to help in recognizing potential problems and artifacts. A number of basic processing methods are discussed in *Schwarz et al.* (1989), *Larson and Slaughter* (1992), and *Farnham and Meech* (1994). We review these and introduce additional techniques in the following discussion, and present representative enhancements in Fig. 4. As this figure shows, different techniques can produce dramatically different effects, and it is advisable to utilize several different ones on the same image, so that they complement each other and act to create an overall portrayal of all aspects of the coma. This also provides a cross-check to determine if a feature is real or if it was introduced by the processing.

Before introducing the different enhancement techniques, we address a few practical notes regarding their definitions and applications. First, many of the techniques require the "removal" of a radial profile from the observed coma. This removal process can be done via either subtraction or division, with very different results. For example, subtracting a $1/\rho$ profile emphasizes features in the innermost coma, while dividing by this same profile suppresses the innermost coma but dramatically enhances the features further out (compare Figs. 4b and 4c). Second, a number of techniques require that a coma profile be created directly from the comet images themselves. Usually, this involves combining a set of pixels (e.g., all the pixels in a given annulus) to produce a mean value that can then be removed. For these cases, we tend to utilize the term "averaging" of the pixels, but they can be combined by computing the mean, median, or mode of the sample. Again, different results can be obtained in each case. Third, many enhancements utilize radial and/or azimuthal information from the original image to generate profiles. For these situations, it is easiest to work with an image that has been unwrapped

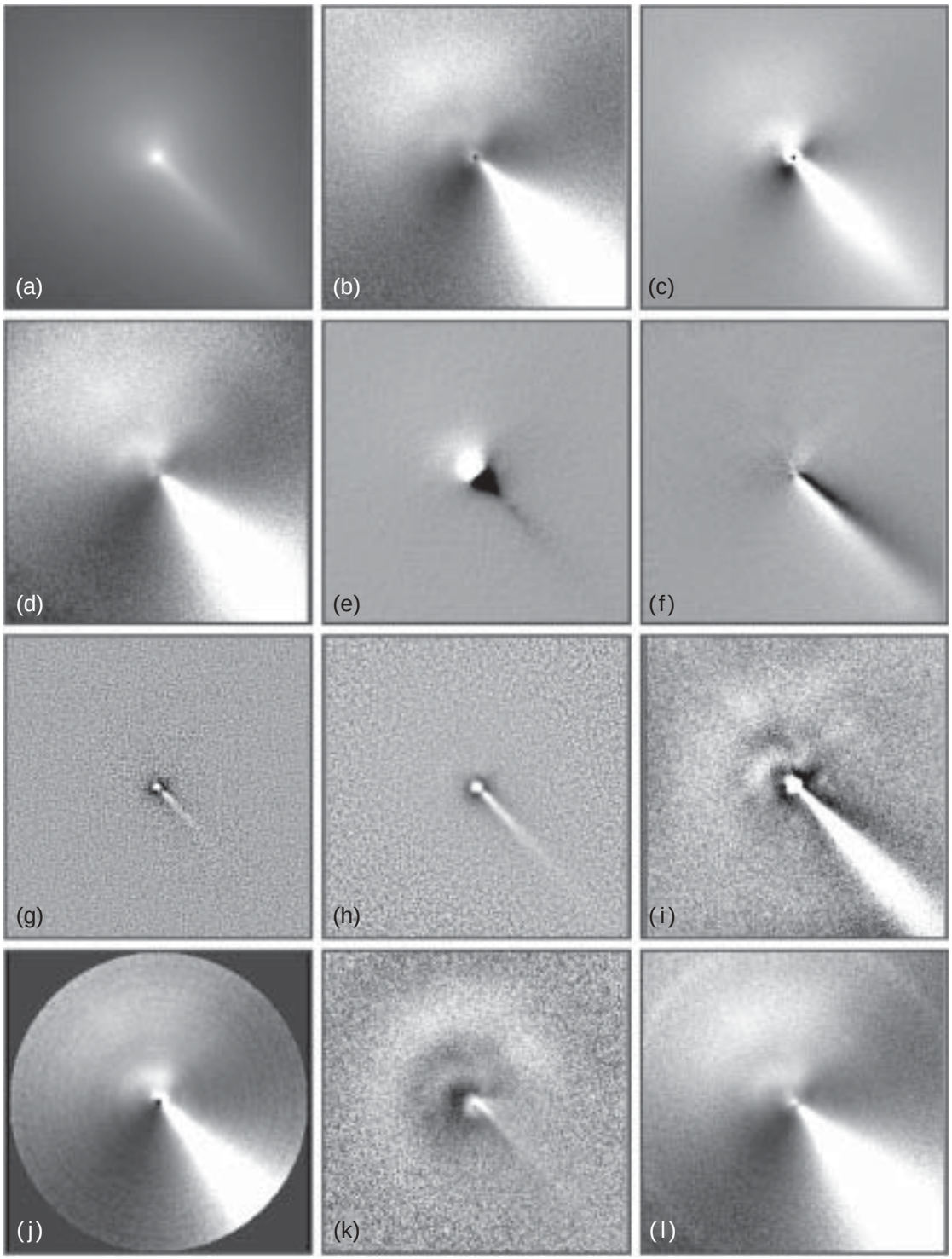

Fig. 4. Comparison of different image enhancement techniques on a common coma image containing three primary features: a broad, diffuse outer arc, an intermediate-scale inner arc, and a narrow, sharply defined tail. These three examples illustrate the type of features revealed by each technique (although different kernel sizes or shifts of different amounts can change the scale of the features that are revealed). Note that some methods enhance the radial tail, others reveal the azimuthal arcs, and some remove the azimuthal variations, while in others it is retained. Although dramatically different results are obtained with the different techniques, it is clear that no single enhancement is ideal for every situation. This emphasizes why multiple techniques should be used to investigate the variety of potential coma features that may be present. **(a)** Original image of Comet Hyakutake (*Schleicher and Woodney,* 2003), displayed with a logarithmic scale to show the straight narrow tail. **(b)** $1/\rho$ profile, divided out. **(c)** $1/\rho$ profile, subtracted out (for comparison, to show how different applications of the same technique can affect the result). **(d)** Azimuthal-averaged profile divided out. **(e)** Linear shift difference with a five-pixel shift in both the vertical and horizontal directions. **(f)** Rotational shift difference with a 10° rotation. **(g)** Laplace filter. **(h)** Unsharp mask with a three-pixel Gaussian smoothing kernel. **(i)** Radial gradient filter. **(j)** Azimuthal renormalization. **(k)** Phase-stacked mask. **(l)** Phase-stacked/azimuthal-averaged profile. Other examples of enhancements **(b)** and **(d)** are shown in Fig. 3.

from the standard rectangular format into a polar format (θ,ρ, where θ is the position angle and ρ is the projected distance from the nucleus). Using the unwrapped image, it is trivial to extract radial and azimuthal information from the rows and columns. The drawback to this process is the need for high-quality unwrapping and rewrapping routines that conserve flux and do not introduce artifacts. Finally, we stress the importance of accurately finding the optocenter of the coma when using many enhancement techniques. Accurate centering, at the fractional pixel level, is crucial when any kind of profile is removed from the coma or when the image is being unwrapped into polar coordinates. Similarly, when multiple images are being combined, it is critical to have them properly registered so the nucleus is in the same position in each frame. For most comets, the central condensation of the continuum provides a suitable reference for the optocenter of both gas and dust images, whereas for comets with little or no dust, the nucleus itself is sometimes visible.

The most benign technique available for searching for features comes from the display process itself. Displaying the image with a log or square root intensity or as a histogram equalization, and then adjusting the contrast stretch, will often reveal a significant amount of detail. This is a straightforward method that is available as a standard option on most display packages and tends to work well. Because there is no manipulation of the data, and hence no way to introduce artifacts, any features that are seen are likely to be real. In addition, once a feature has been identified using another technique, it can usually be detected in the original image if the display is set correctly. For this reason, it is a good idea to return to the unprocessed image to confirm the existence of any features found using the more aggressive enhancement methods.

6.2.1. Removal of simple profiles. The most basic level of processing uses a simple profile to remove the bulk coma shape from the observed image. For the continuum, a logical first choice is a 1/ρ profile, in which the brightness falls off as the inverse of the projected distance from the nucleus. This is the canonical shape of a coma produced by steady-state isotropic emission of dust. (An analogous shape for gas images would be a Haser model profile.) The resulting image highlights the deviations of the observed coma from the idealized one. Not only is this an easy enhancement to apply, but it is fairly benign and it makes the interpretation of the morphology relatively straightforward because the extracted profile is smooth and its shape is known. A slightly more complex technique, based on the same principle, uses the observed coma, gas or dust, to create a profile from the comet itself. By averaging azimuthally around the optocenter (easily done from the polar format image) a radial profile that closely matches the shape of the real coma can be created. The main problem with this technique is that strong arc-shaped features or bright stars may introduce bumps into the profile, which can then produce artifacts in the enhanced image. To avoid this, it may be necessary to remove the stars before computing the average profile and/or radially smooth the profile to suppress any arc residuals; in other cases, using a median rather than an average of the annulus pixels may suffice.

6.2.2. Edge detection techniques. Another type of enhancement is the edge detection technique (EDT), which covers a large family of routines. These tend to be very popular because they are easy to use, require little effort to develop, and dramatically increase the contrast of some features. The first group of edge detectors includes derivative routines such a linear shift differencing (*Klinglesmith,* 1981; *Wood and Albrecht,* 1981) or rotational shift differencing (*Larson and Sekanina,* 1984), where a copy of the image is shifted or rotated and then subtracted from the original. Features that are revealed in this process are a function of the size and direction of the shift, so several applications should be used to look for features at different spatial scales and in different orientations. A powerful benefit of the rotational shift is that a rotation around the optocenter will produce small shifts near the nucleus, where features tend to be small and well-defined, and increasingly larger shifts at larger distances, where the features spread out and become more diffuse. This minimizes the number of applications needed. Another technique, the temporal derivative, uses the ratio of two images obtained at different times to reveal changes in the features as a function of time. This technique is frequently used for work with plasma tails where features change rapidly. There are situations where the temporal derivative can be used over longer timescales (e.g., night to night), but the approach should be used cautiously because other factors, including seeing variations and changes in the viewing geometry, can also affect the appearance of the coma. Next is the color derivative, which, although not an EDT, we include here for completeness. In this method, the ratio of two images obtained at different wavelengths (usually from two different continuum filters) shows spatial color variations in the coma. This is useful for procedures such as comparing the particle size information in a jet to that in the rest of the coma. This derivative should be used with care, however, because gas contamination, poor flat fielding, or residual sky background can produce misleading results, and so high-quality, decontaminated data are necessary for accurate results.

The next group of edge-detection enhancements includes spatial filters, such as the Laplace filter and other procedures in which a kernel is convolved with the image (e.g., *Richards,* 1993). It also includes unsharp masking (e.g., *Sekanina,* 1978), in which a copy of an image is digitally smoothed and the lower-resolution version removed from the original. These techniques tend to be easy to use and are very useful for exploring whether or not features are present. However, if measurements are to be obtained from the processed image, then edge-finding routines should be avoided for a number of reasons. First, the enhanced features are dependent on the size and shape of the filter that is applied, which in turn affects the interpretation of the result. When using unsharp masking, for example, smoothing the image with a Gaussian filter produces a result very

different from what is obtained with a square filter. Second, EDTs are specifically designed to identify edges or discontinuities. Thus, positions obtained from an EDT-enhanced image may not be accurate if the measurements are intended to represent the center of a feature (as is usually the case when the positions are used as input for coma models). Third, these techniques are very harsh and remove a significant amount of information about the coma, which is why they produce high-contrast features. Fourth, this same harshness means that EDTs are more prone to introducing artifacts, especially near the nucleus where the bright central peak dominates. Artifacts are also more common in regions where multiple features overlap and can interact with the convolution filter in an unpredictable manner.

6.2.3. Azimuthal renormalization and radial gradient filter. We now turn to enhancement techniques that are somewhat more involved to create or apply. The first of these is azimuthal renormalization (*A'Hearn et al.*, 1986a), in which the coma is divided into a series of annuli and the pixel intensities in each annulus are rescaled to a common minimum and maximum. Again, this is a simple procedure to perform using the polar format image. The result is effective for removing the central peak, although it also removes much of the relative brightness information. Its strength lies in its usefulness for showing radial features that rapidly fade with distance. Another, more-intricate technique that is presently not widely available is the radial gradient spatial filter (S. M. Larson, personal communication, 2002). This routine uses the basic principles of a convolution filter, but varies the size of the kernel as a function of the distance from the nucleus. The result has the same benefits as the rotational shift removal, in that the enhancements are optimized to reveal small features near the nucleus and increasingly larger features at greater distances, but unlike the rotational shift, it enhances azimuthal as well as radial features (Fig. 4i).

6.2.4. Image sequences and temporal image enhancements. Relating to the following enhancement techniques is another tool that can be useful for understanding and interpreting complicated features. Given a sequence of images uniformly spaced in time, a "movie" of the comet motions can be created. With these sequences, the evolution of the coma and the motions of the features can be followed more clearly. Furthermore, if the features have a periodic nature (e.g., consecutive arcs representing successive rotations of the nucleus) and the viewing geometry varies slowly with respect to the rotation period, then it may be possible to phase images from different rotational cycles to simulate a full rotation. If so, then movies can be created, even if the comet was only observed for short periods on any given night during an observing run.

Unfortunately, most standard enhancement techniques are not optimally suited for use on a sequence of images. For example, an unsharp mask can only be applied to the individual frames in any sequence, but due to temporal changes in the features, the shape removed by the mask will be different for each image. This makes it difficult to directly compare the results. To avoid this problem, it makes sense to enhance the images by removing the same bulk coma shape from each frame. Again, a standard profile (e.g., $1/\rho$) can be assumed or one can be created from the comet itself. In the latter case, however, the profile should be derived using all the images in the sequence so that it incorporates not only spatial variations in the the coma, but temporal ones as well. This was done in an analysis of the CN jets in Comet Halley (*Schulz and A'Hearn,* 1995) in which a series of images were combined to produce an averaged shape that was then removed from the individual frames.

In this same vein, we developed and tested a set of procedures for use in situations where the rotation period is known and is well covered by observations. We found that taking a sequence of images, uniformly spaced throughout the rotation sequence, and averaging them together works well to create a template for removing the bulk coma. The averaging process smooths out temporal changes in the features, so that when the template is removed from each image, any moving features are highlighted. Because the template is created by combining images throughout a rotational phase, we refer to this technique as the phase-stacked mask. In essence, this procedure is a straightforward mask removal, which means that it is relatively benign, it is very good for enhancing faint structure, it can be used to enhance any image obtained throughout the rotation (e.g., it is not restricted to those that were used to create the mask), and any features that are revealed are not likely to have their positions shifted. Like many other techniques that use a coma shape derived from the comet itself, most of the intensity information is lost, including any azimuthal asymmetries. As is discussed later, these asymmetries can provide important constraints on the coma models, so it may be desirable to retain the information. To avoid removing the asymmetries, the procedure can be taken a step further by computing the average azimuthal profile from the phase-stacked mask, to produce a phase-stacked/azimuthal-averaged profile. Removal of this profile from the individual images then enhances the features, while still preserving the original azimuthal asymmetries.

These two phase-averaging techniques, used together, have proven to be very useful in analyses of images of Comets Hale-Bopp and Hyakutake (*Farnham et al.*, 1998b; *Schleicher and Woodney,* 2003). Unfortunately, they have drawbacks that limit the number of objects on which they can be used: They are time-consuming to apply, the comet's rotation period must be known, and multiple images with good phase coverage are needed to smooth out the features. If good temporal coverage is not available, combining the images from different phases may leave residual features in the profile that can again introduce artifacts when the template is used to enhance an image (as is the case for any of the temporal-averaged techniques). Fortunately, most of these residual features can be removed from the averaged profile by applying a smoothing spline function in the radial direction, which minimizes the effect of poor phase coverage. Although this may slightly change the shape of

the coma template, it can still be effectively used to enhance the original images to reveal temporal changes in the coma.

6.3. Quantitative Measurements

Once features have been identified in the coma, with or without the use of enhancements, their qualitative appearance must be converted into quantitative measurements that can be used as constraints for coma models. Depending on the types of features present and the requirements of the model, different measurements are possible. For predominantly radial features, the position angle (PA) of the feature is the most useful measurement, although if some curvature is present, then it may also be necessary to specify at what distance the PA was obtained. Positions of arcs and spirals are usually quantified by measuring the cometocentric distance at a number of different PAs. When making these measurements, the center or brightest point of the jet is the preferred reference location, because models are more likely to reliably reproduce the bright central peak of the jet than its edge. Characterization can also include measurements of other properties, such as the width of the feature, which is often quoted as the full-width at half-maximum (FWHM) above the background. Although this type of measurement can be difficult (and may require additional information if the feature is not symmetric about the center), it provides valuable information about the dispersion of the material in the jets. For the gas species it may also provide information about the relative velocities of the parent and daughter species.

As with the enhancement procedures, it is useful to utilize the polar format image, as well as the rectangular image, for making certain spatial measurements. The polar format not only provides a different perspective for looking at the data (cf. *Schwarz et al.*, 1997; *Samarasinha and Mueller*, 2002), but PAs and distances are directly measurable from the rows and columns. Also, whenever possible, measurements should be obtained from multiple images. If the features are stationary, then the additional measurements will improve the uncertainties; if they move, then the additional measurements give positions as a function of time, and result in a quantitative measure of the motion and thereby constrain the projected velocity of the feature.

Another form of quantitative measurement that can be used to constrain models is the brightness of the coma and morphological features. The brightnesses of different jets can be used to find the relative strengths of their sources, while the amount of material coming from the active areas can be compared to that in the isotropic background. Using the brightness in this manner requires that, if any image enhancement techniques at all are used, then they must be very benign so that relevant brightness information is not lost. Furthermore, to get a proper comparison of the brightness levels, contributions from undesired species must be removed from the images. Thus, not only must continuum be removed from the gas images, but also contamination from other gas species (e.g., the wing of C_3 in the CN filter), which requires an accurate calibration of the images. Ultimately, it may be possible to use the calibrated images to constrain the models sufficiently well to determine gas and/or dust release rates as a function of location on the nucleus.

6.4. Rotation Periods

Many comets exhibit features that are observed to regularly repeat with time. These repetitious structures are a signature of the rotation of the nucleus and under the proper conditions, they can be used to measure the rotation period. Repeating features can include concentric arcs, a ray that oscillates back and forth, or any structure or outburst that appears at regular intervals. These manifestations reflect either the changing production rates as active regions rotate into and out of sunlight or the changing direction of the emission as the nucleus spins, and thus can be used to derive the rotation period. Furthermore, regular repetitions in the morphology suggest that the nucleus is in or near a state of principal axis rotation. (Although long-term precession or complex rotation may be present in some comets, they cannot be addressed if they are not evident in the available observations.) There are exceptions to this rule, including Comet Halley, which exhibits periodic variations, even though it is in a state of complex rotation (*Belton et al.*, 1991).

The most straightforward means of measuring the rotation period is to use a sequence of images that span a full rotation of the nucleus, as was done for Comets Halley (*Samarasinha et al.*, 1986; *Hoban et al.*, 1988), Swift-Tuttle (*Boehnhardt and Birkle*, 1994; *Fomenkova et al.*, 1995), Hyakutake (*Schleicher et al.*, 1998b), and Hale-Bopp (*Sarmecanic et al.*, 1997; *Jorda et al.*, 1999). The period is simply the time that it takes for the feature to reappear in the same place it was at the start of the sequence. Unfortunately, this requires an observing window that permits good temporal coverage throughout a full rotation period, which can be rare for comets. In the examples noted above, Hale-Bopp was bright enough that distinct features could be seen in infrared measurements obtained during the day; Hyakutake passed near Polaris and, for northern hemisphere observers, was observable all night during its closest approach to Earth; and Halley and Swift-Tuttle have rotation periods that span several days, so coverage over many nights provided sufficient sampling to follow the rotation.

If the comet is only observable for short periods, then other methods must be used to derive the rotation period from the features. One method is to phase images from night to night, as discussed above, to determine how long it takes for a feature to repeat. This requires an understanding of how much a feature moves from one night to the next to avoid converging on a false alias of the period, but motions can usually be constrained with observations spanning an hour or two. In the case of Comet Hale-Bopp, the motion of an arc during 2 h of observations was sufficient to show that the arc would repeat about twice per day (i.e., the nucleus had a rotation period of approximately 12 h, rather than 24 or 8 if the arc repeated once or three times respec-

tively). With this constraint, images from several nights could be utilized to determine a more precise rotation period of 11.3 h (*Lecacheux et al.,* 1997; *Mannucci and Tozzi,* 1997; *Licandro et al.*, 1998; *Farnham et al.*, 1998a; *Warell et al.*, 1999). If temporal coverage is minimal, an alternative, although less reliable, method can be used to constrain the rotation period. Using the curvature of a jet and an estimate of the outflow velocity, the spin rate of the nucleus may be found (e.g., *Larson and Sekanina,* 1984; *Watanabe,* 1987; *Boehnhardt et al.,* 1992). Unfortunately, a lack of phase coverage means that assumptions must be made about the projection effects and outflow velocities (or they must be constrained in some independent manner). If the assumptions are not valid, then the results may have significant errors.

Finally, in quoting a rotation period, it should be specified as to which type has been determined: sidereal, solar, or synodic. The sidereal rotation period, which is the most desired but not always the one measured, is the time needed for the nucleus to rotate once with respect to the stars. The solar rotation period is the time it takes for one full rotation with respect to the Sun. Since most morphological features are directly related to the amount of sunlight illuminating an active region, this is probably the most common type of period measured from coma morphology. The solar rotation period is also commonly referred to as the synodic rotation period, in a manner analogous to that used with planets in the solar system. Unfortunately, the term synodic period is also often used, particularly in asteroid studies, for the time needed for one rotation of a body with respect to Earth. Therefore, it is important to define which type of synodic period is meant for any particular usage. The differences between these three periods are usually small, but in some circumstances, they may not be negligible and understanding exactly what is being measured may be important. For example, Comet Hyakutake's solar rotation period was measured sufficiently accurately as to be distinguishable from the sidereal period determined from Monte Carlo modeling of the dust jets during the comet's close approach to Earth. The difference of 0.0004 d between the two periods was completely consistent with the expected difference, based on the model pole orientation and the position of the comet in its orbit (*Schleicher and Woodney,* 2003).

6.5. Modeling Morphological Features

We now turn to methods that are used for inferring additional properties of the nucleus from the coma morphology. In certain circumstances, properties can be determined directly from measurements, without the need for models. An excellent example of this is Comet Borrelly, whose strongest source emits material in a straight jet that is aligned with the nucleus' spin axis. Given this configuration, the apparent position of the jet on different dates can be used to determine the orientation of the rotation pole (*Farnham and Cochran,* 2002) [a similar technique was used in an analysis of Hale-Bopp by *Licandro et al.* (1999)]. It is ironic that the jet can be used to determine so much about the spin axis, but because it is at the pole, it contains no information about the rotation period or the direction of spin.

The fortuitous circumstances regarding Comet Borrelly are unusual, however, and for most comets, more intricate models of the coma morphology must be used to extract the nucleus properties. Many different models, both simplistic and intricate, have been introduced to explain the morphology observed in cometary comae. Early models invoked such concepts as using thermal lags to explain the projected direction of a sunward fan on a homogeneous rotating nucleus (*Sekanina,* 1979) and using the dimensions of consecutive arcs along with assumed expansion velocities to compute rotation periods (*Whipple,* 1982). These early models produced mixed results at best, with a number of the test cases being proven wrong by subsequent observations (Borrelly being one notable case). The next generation of models used continuous tracks of jet particles to follow the features produced by emitted material (*Sekanina,* 1981; *Sekanina and Larson,* 1984, 1986; *Massonne,* 1985) and showed promising results. More recently, a variety of different types of models have been presented, for reproducing both dust morphology (cf. *Sekanina,* 1987, 1991; *Sekanina et al.,* 1992; *Combi,* 1994; *Sekanina and Boehnhardt,* 1997; *Fulle et al.,* 1997; *Schleicher et al.,* 1998c; *Samarasinha,* 2000) and gas morphology (cf. *Lederer et al.,* 1997; *Festou and Barale,* 2000). Most of these recent techniques are based on numerical methods or Monte Carlo simulations.

The increase in computing power over the last decade has not only made the Monte Carlo-style techniques very popular, but they are also very powerful and provide a natural approach for simulating particles emitted from a spinning nucleus. In addition to the characteristics already discussed, a number of fundamental nucleus properties can be determined from the morphology, including a comprehensive depiction of the rotation state and the locations and sizes of the active areas. Secondary parameters can also be derived using the results from the primary analysis: With an understanding of the spin properties and source locations, projection effects can be computed, allowing true distances and velocities to be determined; similarly, thermal lags can be found when sources remain active, even after they are no longer illuminated by sunlight; knowledge of the rotation state and production rates (which can be estimated from the solar illumination on the active regions), provides necessary constraints for analyses involving torques and nongravitational forces on the nucleus (*Samarasinha et al.,* 2004; *Yeomans et al.,* 2004); finally, comparisons of models independently derived from the dust and various gas species may reveal potential composition inhomogeneities, if different species originate from different source regions. Under typical circumstances, only a subset of these properties will be determined for any given comet, with the type and quality of the features governing which results can be derived.

When using models to analyze a comet's coma morphology, different researchers are likely to use slightly different approaches, although the fundamental basis will be similar. The following discussion describes the specific techniques

and procedures that we have used in our work with various comets, and although the details may differ somewhat from other researcher's methods, any model should address essentially the same issues. In our work, we use a standard Monte Carlo model that is discussed more fully by *Schleicher and Woodney* (2003) and Farnham and Schleicher (in preparation, 2004). The routine is presently designed to model the motions of the dust grains and can follow up to 10^6 representative particles that are emitted from multiple active areas at different locations and of different sizes (allowing us to model the extended active areas discussed later). The model can also handle radiation pressure and precession of the nucleus, if necessary. Initial calculations are done in the comet's orbital reference frame, from which it is straightforward to determine the orientation of the nucleus, the Sun's position, and other geometric relationships. For each particle, the routine computes the direction in which it was emitted and the distance it has traveled between its emission time and the observation time, which defines its location in cometary coordinates when the comet was observed. After the positions have been computed for all the particles, the results are then transformed to the plane of the sky coordinates as seen from Earth, and the result can be compared to the observed morphology. The nucleus properties that can be found from our model include the rotation period; orientation of the spin axis; direction of rotation; locations, sizes, and relative strengths of multiple active areas; emission velocities; and the average influence of radiation pressure on the dust grains.

In our application of the model, we start by selecting the most obvious and clearly defined feature in an image and use it as a guide throughout the early stages of the modeling. By initially focusing on only the main feature, we can limit the number of free parameters, which reduces the volume of phase space that must be explored. (Typically only four parameters — right ascension and declination of the pole, the rotation period, and the latitude of the primary source — are needed to explore the basic morphology; other parameters, such as the longitude of the source and the ejection velocity, only control the relative phasing and the scale of the coma.) Next, we assign a pole orientation and a location for the main active region and generate a model for those parameters. Comparing the synthetic image to the observed one (specifically, to the positions measured from the images) allows us to adjust the model parameters and rerun the model to improve the fit. This process is iterated until the model parameters converge to produce a good match to the observations. As in any multivariable analysis, there is always a concern that the parameters are unique and that other combinations of parameters cannot be combined to produce equally suitable results. Therefore, to avoid missing any potential solutions, we perform a full grid search of the four main parameters at low resolution. This allows us to map the areas of parameter space where viable models exist, and we can then focus on these areas at higher resolution to converge on the optimum solution. Once the orientation of the spin axis and location of the main source have been constrained, and parameter space has been narrowed, we can introduce additional parameters (new active regions, radiation pressure, etc.) to model other features and help fine tune all the model parameters. This is again done in stages to allow the effects of each addition to be determined.

Given the fact that there will always be at least four free parameters (with the potential of many more), any information that can be used to help narrow down the parameter space is welcome. Frequently, it is possible to use a simple inspection of the morphology to limit parameters, even before detailed modeling begins. For example, the shape of a spiral arc can often be used to set constraints on the parameters. If the spirals extend completely around the nucleus, then Earth must lie within the cone swept out by the active region during a rotation (i.e., the sub-Earth point lies at a higher latitude than the active region). In addition, the shape of the spiral may define the direction of rotation, which will naturally eliminate at least half the potential pole orientations. Finally, if the spiral appears elongated, then the ratio of the short- and long-axis dimensions can provide a constraint on the aspect angle of the pole. Similarly, radial features can also be used to constrain the parameters. A jet that oscillates back and forth in position angle indicates that Earth is outside the cone, and the size of the oscillation can be used to set a limit on the latitude of the source. Furthermore, if the feature is continuously visible, then the center of the oscillation likely represents the projection of the rotation axis on the sky. Even though some parameters can be constrained in this manner, it is a good idea to utilize the modeling process to check that the interpretation of the features is correct and to make sure that the excluded areas of parameter space behave as expected.

Another procedure that can be employed in the analysis is the incorporation of multiple images throughout the comet's apparition (e.g., *Braustein et al.,* 1997; *Vasundhara and Chakraborty,* 1999). Tracking the long-term evolution of the coma makes it possible to generate a comprehensive model for reproducing the general appearance of the coma at any given time. Furthermore, dramatic changes in the morphology can act as benchmarks for deriving the locations of the active regions. For example, the gradual appearance or disappearance of a bright jet can indicate that the subsolar latitude is changing and a source is becoming illuminated or losing its illumination. Observations spanning a significant arc of the orbit may also reveal other factors, such as the times at which Earth crosses into or out of the cone swept out by an active area. These types of information can be used to severely constrain the locations of the source regions, which in turn simplifies the modeling process.

We now address a new complication regarding coma models that was introduced during our studies of Comet Hale-Bopp and has implications for coma models in general. There is an extensive amount of data available for this comet around the time of perihelion and the coma could be studied in detail from March through early May. Exami-

nation of the arcs in any particular Hale-Bopp image from this time frame shows primarily circular features (dust arcs or CN spirals) with little foreshortening in any direction. The rounded shape suggests that the comet's spin axis was pointed in the general direction of Earth, which posed a problem, because the Earth-comet viewing geometry changed by about 90° between March and May. In other words, for the pole to be pointed toward Earth throughout this time frame, the nucleus would have to be in a state of fast precession with the pole tracking Earth — a difficult scenario to accept. The solution to this puzzle was suggested by *Samarasinha* (2000), and involves the size of the active region creating the feature. Normally, jets in a model are assumed to be narrow, if indeed any width at all is specified. This simplifies the models, produces well-defined features, and has been widely accepted because the result usually reflects the appearance of the observed image. Samarasinha suggested that the arcs in Comet Hale-Bopp are not produced by jets only a few degrees wide, but instead are the result of large active regions, spanning tens of degrees in latitude and/or longitude. The effect of these broad jets is to form a partial shell structure that can mimic the planetary nebula effect. In a planetary nebula, the spherical shell appears to be circular because the greatest column density is at the outer edge. Similarly, in Hale-Bopp, the partial shells are seen as arcs that always appear circular, even when the aspect angle changes dramatically (Fig. 5). Another effect of the extended sources is that they can create intricate overlapping structures, which naturally reproduce the appearance of many of the complicated features seen in Hale-Bopp.

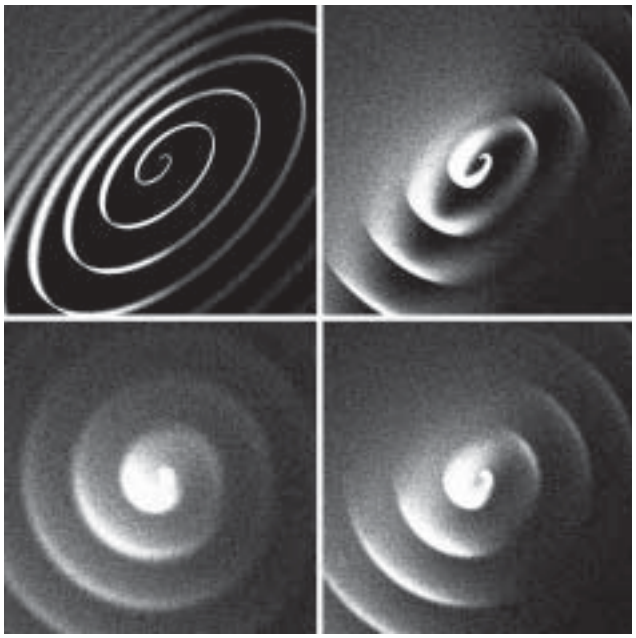

Fig. 5. Sequence of simulated images showing the effects of extended active regions on the appearance of the coma. Clockwise from the upper left, the source regions span angles of 1°, 5°, 15°, and 30°, with all other parameters left unchanged. Notice that for the larger source regions, the arcs are more circular, giving the appearance that Earth lies very close to the spin axis. From *Samarasinha* (2000).

The existence of wide jets makes the coma more difficult to model, not only because it introduces more free parameters, but also because it makes interpretation of the features more difficult. With an extended source, the existence of a complete spiral around the nucleus is no longer a guarantee that Earth lies within the cone formed by the spinning jet. If Earth lies within only a part of the cone produced by the jet, the planetary nebula effect will dominate and full spirals will be observed. Furthermore, as with Hale-Bopp, the rounded arc appearance no longer provides a severe constraint on the aspect angle of the pole. It is clear from these examples that the potential for having extended active regions introduces ambiguities into the constraints that can be set with simple inspection of the coma structure. Thus, in any comprehensive analysis, it is wise to investigate the possibility that broad jets are contributing to the coma morphology, because the differences can have a profound influence on the model results, as it did for Comet Hale-Bopp.

Our final discussion addresses various concerns and considerations to be aware of when applying these models. First, the uniqueness of the solution is foremost when presenting a result, and a global search of parameter space, although tedious and time consuming, may be necessary to rule out other families of solutions. Next, a comprehensive model should reproduce the morphology of the original image, not the enhanced one. When possible, the model should be enhanced with the same methods used on the original image to see how well the two really match. This is not always practical, especially during the global search of parameters, but as the solution converges, the quality of the fit is more critical. Related to this is the principle of determining how good a fit has actually been obtained. Using a mathematical measure of the goodness-of-fit (e.g., a χ^2 fit) is usually not practical because quantifying the difference between the model and the image can be difficult without resorting to time-consuming measurements. Fortunately, pattern matching by eye is very effective for this type of work, especially when the results can be displayed in multiple formats. This argues that both the rectangular and polar versions of the model and the image should be compared. Finally, the role that is played by the background material in the coma should be considered. The bulk shape of the coma (the component that is usually removed in the enhancement process) must come from somewhere, with two possible sources being isotropic emission from the nucleus' surface and diffusion of material outward from the isolated sources. Ideally, this component should be included in the model for completeness, but it is not always clear exactly how to include it or account for it.

As described here, modeling the structures in cometary comae can reveal fundamental properties of the nucleus.

The results that are obtained are inherently important in and of themselves, but they become even more valuable when they are used to set constraints on a variety of other comet studies. We note a few of these, which are discussed in more detail in other chapters of this book. First, understanding the main jet structures in the coma as a function of time helps in interpreting the more intricate effects produced by topography and the gas/dust interactions near the nucleus (*Crifo et al.*, 2004). As discussed earlier, the rotation properties can be used as examples for studies of the rotational dynamics of nuclei (*Samarasinha et al.*, 2004) and, when the locations of the active regions are included, for research related to nongravitational forces (*Yeomans et al.*, 2004). Information about the sizes and locations of the active areas and when they turn on and off provide constraints for studies of normal cometary activity and outbursts (*Prialnik et al.*, 2004; *Boehnhardt*, 2004). Finally, the source activity information and true emission velocities obtained from inner coma models can be used to improve models of the gas dynamics (*Combi et al.*, 2004) and models of the comet's dust tail (*Fulle*, 2004).

7. FUTURE DIRECTIONS

The past two decades have seen vast advances in the capabilities of array detectors, including extended wavelength coverage, particularly in the near-UV, increased quantum efficiencies at all wavelengths, improved noise characteristics, decreased readout times, and larger formats. With these improvements, coma morphology studies have become common, especially for brighter comets, although most such studies have been qualitative in nature; analyses involving absolutely calibrated, continuum-subtracted, and decontaminated gas images are unfortunately still only rarely performed. We hope that the recent introduction of new narrowband filter sets by ESA and NASA, with filter sizes as large as 100 mm for use with large-format CCD cameras, will provide additional incentive to perform more quantitative studies in the future. In any case, newer large-format cameras will certainly provide larger fields-of-view for active comets than previously possible, thereby sampling significantly larger portions of the coma than have been typical in the past. These developments should lead to improved models of the outflow and interaction of dust and gas in comae. However, even with the many ongoing advances in the field of narrowband imaging, we believe that narrowband measurements with conventional photometers will continue to provide very important results regarding the overall chemical composition of comets for many years to come.

The ability to directly intercompare model comae with observations will continue to improve with advances in computing power, permitting large increases in the number of particles used in Monte Carlo-type simulations and more realistic scenarios. Increases in computing power will also allow multivariable minimization routines to be used to explore and constrain the multidimensional parameter space more efficiently. Furthermore, coma models will undergo severe testing, with spacecraft encountering several comets in the near future; these encounters will either validate the modeling procedures that are currently in use, or will prompt their reevaluation.

Finally, narrowband imaging, multiwavelength polarization studies show promise for better understanding the physical properties of dust grains as they move outward from the nucleus. They may answer questions about fragmentation of grains and whether the ambient background of the coma is caused by dispersed grains from jets or by a more homogeneous nucleus component.

Acknowledgments. The authors particularly thank M. A'Hearn, A. Cochran, M. Combi, R. Millis, S. Larson, and N. Samarasinha for innumerable fruitful conversations regarding aspects of the contents of this chapter, as well as the referees for many useful comments and suggestions. We also thank S. Larson for providing the radial gradient filter enhancement of the image of Comet Hyakutake. This work has been made possible due to grants from the National Aeronautics and Space Administration and the National Science Foundation.

REFERENCES

A'Hearn M. F. (1982) Spectroscopy and spectrophotometry of comets at optical wavelengths. In *Comets* (L. L. Wilkening, ed.), pp. 433–460. Univ. of Arizona, Tucson.

A'Hearn M. F. (1983) Photometry of comets. In *Solar System Photometry Handbook* (R. Genet, ed.), pp. 3-1–3-33. Willmann-Bell, Richmond, Virginia.

A'Hearn M. F. (1991) Photometry and polarimetry network. In *The Comet Halley Archive Summary Volume* (A. Sekanina, ed.), pp. 193–235. Jet Propulsion Laboratory, Pasadena.

A'Hearn M. F. and Cowan J. J. (1975) Molecular production rates in Comet Kohoutek. *Astrophys. J., 80*, 852–860.

A'Hearn M. F. and Millis R. L. (1980) Abundance correlations among comets. *Astrophys. J., 85*, 1528–1537.

A'Hearn M. F., Millis R. L., and Birch P. V. (1979) Gas and dust in some recent periodic comets. *Astrophys. J., 84*, 570–579.

A'Hearn M. F., Schleicher D. G., Feldman P. D., Millis R. L., and Thompson D. T. (1984) Comet Bowell 1980b. *Astrophys. J., 89*, 579–591.

A'Hearn M. F., Birch P. V., Feldman P. D., and Millis R. L. (1985) Comet Encke — Gas production and lightcurve. *Icarus, 64*, 1–10.

A'Hearn M. F., Hoban S., Birch P. V., Bowers C., Martin R., and Klinglesmith D. A. III (1986a) Cyanogen jets in Comet Halley. *Nature, 324*, 649–651.

A'Hearn M. F., Birch P. V., and Klinglesmith D. A. III (1986b) Gaseous jets in Comet P/Halley. In *20th ESLAB Symposium on the Exploration of Halley's Comet, Vol. 1* (B. Battrick et al., eds.), pp. 483–486. ESA SP-250, Noordwijk, The Netherlands.

A'Hearn M. F., Millis R. L., Schleicher D. G., Osip D. J., and Birch P. V. (1995) The ensemble properties of comets: Results from narrowband photometry of 85 comets, 1976–1992. *Icarus, 118*, 223–270.

Arpigny C. (1976) Interpretation of comet spectra: A review. In *The Study of Comets* (B. Donn et al., eds.), pp. 797–838. NASA SP-393, Washington, DC.

Baum W. A., Kreidl T. J., and Schleicher D. G. (1992) Cometary grains. *Astrophys. J., 104*, 1216–1225.

Belton M. J. S., Mueller B. E. A., Julian W. H., and Anderson

A. J. (1991) The spin state and homogeneity of Comet Halley's nucleus. *Icarus, 93,* 183–193.

Blamont J. E. and Festou M. (1974) Observation of the comet Kohoutek (1973f) in the resonance light ($A^2\Sigma^+$–$X^2\Pi$) of the OH radical. *Icarus, 23,* 538–544.

Bockelée-Morvan D., Crovisier J., Mumma M. J., and Weaver H. A. (2004) The composition of cometary volatiles. In *Comets II* (M. C. Festou et al., eds.), this volume. Univ. of Arizona, Tucson.

Boehnhardt H. (2004) Split comets. In *Comets II* (M. C. Festou et al., eds.), this volume. Univ. of Arizona, Tucson.

Boehnhardt H. and Birkle K. (1994) Time variable coma structures in comet P/Swift-Tuttle. *Astron. Astrophys. Suppl. Ser., 107,* 101–120.

Boehnhardt H., Vanysek V., Birkle K., and Hopp U. (1992) Coma imaging of comet P/Brorsen-Metcalf at Calar Alto in late July to mid August 1989. In *Asteroids, Comets, Meteors 1991* (A. W. Harris and E. Bowell, eds.), pp. 81–84. Lunar and Planetary Institute, Houston.

Braunstein M., Womack M., Deglman F., Pinnick G., Comstock R., Hoffman P., Aaker G., Faith D., Moore S., Ricotta J., Goldschen M., Wiest A., Modi C., Jacobson A., and Zilka J. (1997) A CCD image archive of Comet C/1995 O1 (Hale-Bopp): Dust expansion velocities. *Earth Moon Planets, 78,* 219–227.

Budding E. (1993) *Introduction to Astronomical Photometry.* Cambridge Univ., Cambridge. 272 pp.

Chernova G. P., Kiselev N. N., and Jockers K. (1993) Polarimetric characteristic of dust particles as observed in 13 comets: Comparison with asteroids. *Icarus, 103,* 144–158.

Cochran A. L. and Cochran W. D. (1991) The first detection of CN and the distribution of CO^+ gas in the coma of Comet P/Schwassmann-Wachmann 1. *Icarus, 90,* 172–175.

Cochran A. L. and Schleicher D. G. (1993) Observational constraints on the lifetime of cometary H_2O. *Icarus, 105,* 235–253.

Cochran A. L., Cochran W. D., Barker E. S., and Storrs A. D. (1991) The development of the CO^+ coma of Comet P/Schwassmann-Wachmann 1. *Icarus, 92,* 179–183.

Combi M. R. (1994) The fragmentation of dust in the innermost comae of comets: Possible evidence from ground-based images. *Astrophys. J., 108,* 304–312.

Combi M. R., Harris W. M., and Smyth W. H. (2004) Gas dynamics and kinetics in the cometary coma: Theory and observations. In *Comets II* (M. C. Festou et al., eds.), this volume. Univ. of Arizona, Tucson.

Cowan J. J. and A'Hearn M. F. (1979) Vaporization of cometary nuclei: Light curves and lifetimes. *Moon and Planets, 21,* 155–171.

Crifo J. F., Fulle M., Kömle N. I., and Szegö K. (2004) Nucleus-coma structural relationships: Lessons from physical models. In *Comets II* (M. C. Festou et al., eds.), this volume. Univ. of Arizona, Tucson.

Farnham T. L. and Cochran A. L. (2002) A McDonald Observatory study of Comet 19P/Borrelly: Placing the Deep Space 1 observations into a broader context. *Icarus, 160,* 398–418.

Farnham T. L. and Meech K. J. (1994) Comparison of the plasma tails of four comets: P/Halley, Okazaki-Levy-Rudenko, Austin and Levy. *Astrophys. J., 91,* 419–460.

Farnham T. L., Schleicher D. G., Ford E., and Blount E. A. (1998a) The rotation period of Comet Hale-Bopp (1995 O1). In *Abstracts for the First International Conference of Comet Hale-Bopp,* p. 16. Tenerife, 1998 February 2–5.

Farnham T. L., Schleicher D. G., and Cheung C. C. (1998b) Rotational variation of the gas and dust jets in Comet Hale-Bopp (1995 O1) from narrowband imaging. *Bull. Am. Astron. Soc., 30,* 1072.

Farnham T. L., Schleicher D. G., Williams W. R., and Smith B. R. (1999) The rotation state and active regions of Comet Hale-Bopp (1995 O1). *Bull. Am. Astron. Soc., 31,* 1120.

Farnham T. L., Schleicher D. G., and A'Hearn M. F. (2000) The HB narrowband comet filters: Standard stars and calibrations. *Icarus, 147,* 180–204.

Feldman P. D., Cochran A. L., and Combi M. R. (2004) Spectroscopic investigations of fragment species in the coma. In *Comets II* (M. C. Festou et al., eds.), this volume. Univ. of Arizona, Tucson.

Festou M. C. and Barale O. (2000) The asymmetric coma of comets. I. Asymmetric outgassing from the nucleus of Comet 2P/Encke. *Astrophys. J., 119,* 3119–3132.

Fomenkova M. N., Jones B., Pina R., Puetter R., Sarmecanic J., Gehrz R., and Jones T. (1995) Mid-infrared observations of the nucleus and dust of Comet P/Swift-Tuttle. *Astrophys. J., 110,* 1866–1957.

Fulle M. (2004) Motion of cometary dust. In *Comets II* (M. C. Festou et al., eds.), this volume. Univ. of Arizona, Tucson.

Fulle M., Milani A., and Pansecchi L. (1997) Tomography of a sunward structure in the dust tail of comet 19P/Borrelly. *Astron. Astrophys., 321,* 338–342.

Hanner M. S. and Tokunaga A. T. (1991) Infrared techniques for comet observations. In *Comets in the Post-Halley Era, Vol. 1* (R. L. Newburn Jr. et al., eds.), pp. 67–91. Kluwer, Dordrecht.

Henden A. A. and Kaitchuck R. H. (1982) *Astronomical Photometry.* Van Nostrand Reinhold, New York. 392 pp.

Hoban S., Samarasinha N. H., A'Hearn M. F., and Klinglesmith D. A. (1988) An investigation into periodicities in the morphology of CN jets in comet P/Halley. *Astron. Astrophys., 195,* 331–337.

Howell S. B., ed. (1992) *Astronomical CCD Observing and Reduction Techniques.* ASP Conference Series 23, Astronomical Society of the Pacific, San Francisco. 329 pp.

Howell S. B. (2000) *Handbook of CCD Astronomy.* Cambridge Univ., Cambridge. 164 pp.

International Halley Watch (1995) *Comet Halley Archive, Vol. 22.* USA-NASA-IHW-HAL-0022, Small Bodies Node, Univ. of Maryland, College Park (CD-ROM).

Ip W.-H. (2004) Global solar wind interaction and ionospheric dynamics. In *Comets II* (M. C. Festou et al., eds.), this volume. Univ. of Arizona, Tucson.

Jacoby G. H., ed. (1990) *CCDs in Astronomy.* ASP Conference Series 8, Astronomical Society of the Pacific, San Francisco. 407 pp.

Jewitt D. (1991) Cometary photometry. In *Comets in the Post-Halley Era, Vol. 1* (R. L. Newburn Jr. et al., eds.), pp. 19–65. Kluwer, Dordrecht.

Jewitt D. C. and Meech K. J. (1987) Surface brightness profiles of 10 comets. *Astrophys. J., 317,* 992–1001.

Jorda L., Rembor K., Lecacheux J., Colom P., Colas F., Frappa E., and Lara L. M. (1999) The rotational parameters of Hale-Bopp (Comet C/1995 O1) from observations of the dust jets at Pic du Midi Observatory. *Earth Moon Planets, 77,* 167–180.

Kim S. J., A'Hearn M. F., and Cochran W. D. (1989) NH emissions in comets — fluorescence vs. collisions. *Icarus, 77,* 98–108.

Kiselev N. N. and Chernova G. P. (1981) Phase functions of polarization and brightness and the nature of cometary atmosphere

particles. *Icarus, 48,* 473–481.

Klinglesmith D. A. (1981) The interactive astronomical data analysis facility — image enhancement techniques to Comet Halley. In *Modern Observational Techniques for Comets: Proceedings of a Workshop held at Goddard Space Flight Center, Greenbelt, Maryland, on October 22–24, 1980* (J. C. Brandt et al., eds.), pp. 223–231. JPL Publication No. 81-68.

Kolokolova L., Jockers K., Chernova G., and Kiselev N. (1997) Properties of cometary dust from color and polarization. *Icarus, 126,* 351–361.

Kolokolova L., Hanner M. S., Levasseur-Regourd A.-C., and Gustafson B. Å. S. (2004) Physical properties of cometary dust obtained using their light scattering and emission. In *Comets II* (M. C. Festou et al., eds.), this volume. Univ. of Arizona, Tucson.

Lamy P. L., Toth I., Fernández Y. R., and Weaver H. A. (2004) The sizes, shapes, albedos, and colors of cometary nuclei. In *Comets II* (M. C. Festou et al., eds.), this volume. Univ. of Arizona, Tucson.

Larson S. M. and Sekanina Z. (1984) Coma morphology and dust-emission pattern of periodic Comet Halley. I — High-resolution images taken at Mount Wilson in 1910. *Astrophys. J., 89,* 571–578.

Larson S. M. and Slaughter C. D. (1992) Evaluating some computer enhancement algorithms that improve the visibility of cometary morphology. In *Asteroids, Comets, Meteors 1991* (A. W. Harris and E. Bowell, eds.), pp. 337–343. Lunar and Planetary Institute, Houston.

Larson S. M., Sekanina Z., and Rahe J. (1991) Near-nucleus studies network. In *The Comet Halley Archive Summary Volume* (A. Sekanina, ed.), pp. 173–191. Jet Propulsion Laboratory, Pasadena.

Larson S. M., Hergenrother C. W., and Brandt J. C. (1997) The spatial and temporal distribution of CO^+ and CN in C/1995 O1 (Hale-Bopp). *Bull. Am. Astron. Soc., 29,* 1036.

Le Borgne J. F., Leroy J. L., and Arnaud J. (1987) Polarimetry of visible and near-UV molecular bands: Comets P/Halley and Hartley-Good. *Astron. Astrophys., 173,* 180–182.

Lecacheux J., Jorda L., and Colas F. (1997) *Comet C/1995 O1 (Hale-Bopp).* IAU Circular No. 6560.

Lederer S. M., Campins H, Osip D. J., and Schleicher D. G. (1997) Gaseous jets in Comet Hale-Bopp (1995 O1). *Earth Moon Planets, 78,* 131–136.

Levasseur-Regourd A.-C. (1999) Polarization of light scattered by cometary dust particles: Observations and tentative interpretations. *Space Sci. Rev., 90,* 163–168.

Licandro J., Bellot Rubio L. R., Boehnhardt H., Casas R., Goetz B., Gomez A., Jorda L., Kidger M. R., Osip D., Sabalisck N., Santos P., Serr-Ricart M., Tozzi G. P., and West R. (1998) The rotation period of C/1995 O1 (Hale-Bopp). *Astrophys. J. Lett., 501,* L221.

Licandro J., Bellot Rubio L. R., Casas R., Gomez A., Kidger M. R., Sabalisk N., Santos-Sanz P., Serra-Ricart M., Torres-Chico R., Oscoz A., Jorda L., and Denicolo G. (1999) The spin axis position of C/1995 O1 (Hale-Bopp). *Earth Moon Planets, 77,* 199–206.

Mannucci F. and Tozzi G.P. (1997) *Comet C/1995 O1 (Hale-Bopp).* IAU Circular No. 6575.

Massonne L. (1985) Coma morphology and dust emission pattern of Comet Halley. *Adv. Space Res., 5,* 187–196.

Meech K. J. and Jewitt D. C. (1987) Observation of comet P/Halley at minimum phase angle. *Astron. Astrophys., 187,* 585–593.

Meier R., Wellnitz D., Kim S. J., and A'Hearn M. F. (1998) The NH and CH bands of Comet C/1996 B2 (Hyakutake). *Icarus, 136,* 268–279.

Meisel D. D. and Morris C. S. (1982) Comet head photometry: Past, present and future. In *Comets* (L. L. Wilkening, ed.), pp. 413–432. Univ. of Arizona, Tucson.

Millis R. L. and Schleicher D. G. (1986) Rotational period of comet Halley. *Nature, 324,* 646–649.

Millis R. L., A'Hearn M. F., and Thompson D. T. (1982) Narrow-band photometry of Comet P/Stephan-Oterma and the back-scattering properties of cometary grains. *Astrophys. J., 87,* 1310–1317.

Mueller B. E. A., Samarasinha N. H., and Belton M. J. S. (1999) Imaging of the structure and evolution of the coma morphology of Comet Hale-Bopp (C/1995 O1). *Earth Moon Planets, 77,* 181–188.

Ney E. P. (1982) Optical and infrared observations of bright comets in the range 0.5 microns to 20 microns. In *Comets* (L. L. Wilkening, ed.), pp. 413–432. Univ. of Arizona, Tucson.

O'Dell C. R. and Osterbrock D. E. (1962) Emission-band and continuum photometry of Comet Seki (1961f). *Astrophys. J., 136,* 559–566.

Osborn W., A'Hearn M. F., Carsenty U., Millis R. L., Schleicher D. G., Birch P. V., Moreno H., and Gutierrez-Moreno A. (1990) Standard stars for photometry of comets. *Icarus, 88,* 228–245.

Philip A. G. D., Janes K. A., and Upgren A. R., eds. (1995) *New Developments in Array Technology and Applications.* IAU Symposium 167, Kluwer, Dordrecht. 397 pp.

Prialnik D., Benkhoff J., and Podolak M. (2004) Modeling the structure and activity of comet nuclei. In *Comets II* (M. C. Festou et al., eds.), this volume. Univ. of Arizona, Tucson.

Randall E. E., Schleicher D. G., Ballou R. G., and Osip D. J. (1992) Observational constraints on molecular scalelengths and lifetimes in comets. *Bull. Am. Astron. Soc., 24,* 1002.

Richards J. A. (1993) *Remote Sensing Digital Image Analysis: An Introduction.* Springer-Verlag, New York. 340 pp.

Samarasinha N. H. (2000) Coma morphology due to an extended active region and implications for the spin state of Comet Hale-Bopp. *Astrophys. J. Lett., 529,* L107–L110.

Samarasinha N. H. and Mueller B. E. A. (2002) Spin axis direction of Comet 19P/Borrelly based on observations from 2000 and 2001. *Earth Moon Planets, 90,* 473–482.

Samarasinha N. H., A'Hearn M. F., Hoban S., and Klinglesmith D. A. III (1986) CN jets of Comet P/Halley: Rotational properties. In *20th ESLAB Symposium on the Exploration of Halley's Comet, Vol. 1* (B. Battrick et al., eds), pp. 487–491. ESA SP-250, Noordwijk, The Netherlands.

Samarasinha N. H., Mueller B. E. A., and Belton M. J. S. (1999) Coma morphology and constraints on the rotation of Comet Hale-Bopp (C/1995 O1). *Earth Moon Planets, 77,* 189–198.

Samarasinha N. H., Mueller B. E. A., Belton M. J. S., and Jorda L. (2004) Rotation of cometary nuclei. In *Comets II* (M. C. Festou et al., eds.), this volume. Univ. of Arizona, Tucson.

Sarmecanic J. R., Osip D. J., Fomenkova M. N., and Jones B. (1997) *Comet C/1995 O1 (Hale-Bopp).* IAU Circular No. 6600.

Schleicher D. G. (1983) The fluorescence of cometary OH and CN. Ph.D. dissertation, Univ. of Maryland, College Park.

Schleicher D. G. and A'Hearn M. F. (1988) The fluorescence of cometary OH. *Astrophys. J., 331,* 1058–1077.

Schleicher D. G. and Osip D. J. (2002) Long and short-term photometric behavior of Comet Hyakutake (1996 B2). *Icarus, 159,* 210–233.

Schleicher D. G. and Woodney L. M. (2003) Analysis of dust

coma morphology of Comet Hyakutake (1996 B2) near perigee: Outburst behavior, jet motion, source region locations, and nucleus pole orientation. *Icarus, 162,* 190–213.

Schleicher D. G., Millis R. L., and Birch P. V. (1987) Photometric observations of Comet P/Giacobini-Zinner. *Astron. Astrophys., 187,* 531–538.

Schleicher D. G., Millis R. L., Osip D. J., and Birch P. V. (1991) Comet Levy (1990c): Groundbased photometric results. *Icarus, 94,* 511–523.

Schleicher D. G., Millis R. L., and Birch P. V. (1998a) Narrowband photometry of Comet P/Halley: Variation with heliocentric distance, season, and solar phase angle. *Icarus, 132,* 397–417.

Schleicher D. G., Millis R. L., Osip D. J., and Lederer S. M. (1998b) Activity and the rotation period of Comet Hyakutake (1996 B2). *Icarus, 131,* 233–244.

Schleicher D. G., Farnham T. L., Smith B. R., Blount E. A., Nielsen E., and Lederer S. M. (1998c) Nucleus properties of Comet Hale-Bopp (1995 O1) based on narrowband imaging. *Bull. Am. Astron. Soc., 30,* 1063.

Schleicher D. G., Farnham T. L., Williams W. R., Smith B. R., and Cheung C. C. (1999) Modeling the rotational morphology of gas and dust jets in Comet Hale-Bopp (1995 O1) at perihelion. *Bull. Am. Astron. Soc., 31,* 1128.

Schleicher D. G, Woodney L. M., and Millis R. L. (2003) Comet 19P/Borrelly at multiple apparitions: Seasonal variations in gas production and dust morphology. *Icarus, 162,* 415–442.

Schmidt M. and van Woerden H. (1957) The intensity distribution of molecular bands in the coma of Comet Mrkos 1955e. *Liege Inst. d'Ap. Reprint No. 386,* pp. 102–111. Liege, Belgium.

Schulz R. and A'Hearn M. F. (1995) Shells in the C_2 coma of Comet P/Halley. *Icarus, 115,* 191–198.

Schulz R., A'Hearn M. F., Birch P. V., Bowers C., Kempin M., and Martin R. (1993) CCD imaging of Comet Wilson (1987VII) — A quantitative coma analysis. *Icarus, 104,* 206–225.

Schulz R., Stüwe J. A., Tozzi G. P., and Owens A. (2000) Optical analysis of an activity outburst in comet C/1995 O1 (Hale-Bopp) and its connection to an X-ray outburst. *Astron. Astrophys., 361,* 359–368.

Schwarz G., Cosmovici C., Mack P., and Ip W. (1989) Image processing techniques for gas morphology studies in the coma of Comet Halley. *Adv. Space Res., 9,* 217–220.

Schwarz G., Cosmovici C. B., Crippa R., Guaita C., Manzini F., and Oldani V. (1997) Comet Hale-Bopp: Evolution of jets and shells during March 1997. *Earth Moon Planets, 78,* 189–195.

Sekanina Z. (1978) Comet West 1976. VI — Discrete bursts of dust, split nucleus, flare-ups, and particle evaporation. *Astrophys. J., 83,* 1675–1680.

Sekanina Z. (1979) Fan-shaped coma, orientation of rotation axis, and surface structure of a cometary nucleus. I — Test of a model on four comets. *Icarus, 37,* 420–442.

Sekanina Z. (1981) Distribution and activity of discrete emission areas on the nucleus of periodic Comet Swift-Tuttle. *Astrophys. J., 86,* 1741–1773.

Sekanina Z. (1987) Anisotropic emission from comets: Fans versus jets. 1: Concept and modeling. In *Proceedings of the International Symposium on the Diversity and Similarity of Comets* (E. J. Rolfe et al., eds.) pp. 315–322. ESA SP-278, Noordwiijk, The Netherlands.

Sekanina Z. (1991) Randomization of dust-ejecta motions and the observed morphology of cometary heads. *Astrophys. J., 102,* 1870–1878.

Sekanina Z. and Boehnhardt H. (1997) Dust morphology of Comet Hale-Bopp (C/1995 O1). II. Introduction of a working model. *Earth Moon Planets, 78,* 313–319.

Sekanina Z. and Larson S. M. (1984) Coma morphology and dust-emission pattern of periodic Comet Halley. II — Nucleus spin vector and modeling of major dust features in 1910. *Astrophys. J., 89,* 1408–1425.

Sekanina Z. and Larson S. M. (1986) Coma morphology and dust-emission pattern of periodic Comet Halley. IV — Spin vector refinement and map of discrete dust sources for 1910. *Astrophys. J., 92,* 462–482.

Sekanina Z., Larson S. M., Hainaut O., Smette A., and West R. M. (1992) Major outburst of periodic Comet Halley at a heliocentric distance of 14 AU. *Astron. Astrophys., 263,* 367–386.

Sen A. K., Joshi U. C., and Deshpande M. R. (1989) Molecular band polarization in comet P/Halley. *Astron. Astrophys., 217,* 307–310.

Sterken C. and Manfroid J. (1992) *Astronomical Photometry: A Guide.* Kluwer, Dordrecht. 272 pp.

Tatum J. B. and Gillespie M. I. (1977) The cyanogen abundance of comets. *Astrophys. J., 218,* 569–572.

Vanysek V. (1976) Photometry of the cometary atmosphere: A review. In *The Study of Comets, Part I* (B. Donn et al., eds.), pp. 1–27. NASA SP-393, Washington, DC.

Vasundhara R. and Chakraborty P. (1999) Modeling of jets from Comet Hale-Bopp (C/1995 O1): Observations from the Vainu Bappu Observatory. *Icarus, 140,* 221–230.

Warell J., Lagerkvist C.-I., and Lagerros J. S. V. (1999) Dust continuum imaging of C/1995 O1 (Hale-Bopp): Rotation period and dust outflow velocity. *Astron. Astrophys. Suppl. Ser., 136,* 245–256.

Watanabe J.-I. (1987) The rotation of Comet 1983 VII IRAS-Araki-Alcock. *Publ. Astron. Soc. Japan, 39,* 485–503.

Wehinger P. A., Wyckoff S., Herbig G. H., Herzberg G., and Lew H. (1974) Identification of H_2O^+ in the tail of Comet Kohoutek (1973f). *Astrophys. J. Lett., 190,* L43–L46.

Whipple F. L (1982) The rotation of cometary nuclei. In *Comets* (L. L. Wilkening, ed.), pp. 227–250. Univ. of Arizona, Tucson.

Wood H. J. and Albrecht R. (1981) Outburst and nuclear breakup of Comet Halley — 1910. In *Modern Observational Techniques for Comets: Proceedings of a Workshop held at Goddard Space Flight Center, Greenbelt, Maryland, on October 22–24, 1980* (J. C. Brandt et al., eds.), pp. 216–219. JPL Publication No. 81-68.

Woodney L. M., A'Hearn M. F., Schleicher D. G., Farnham T. L., McMullin J. P., Wright M. C., Veal J. M., Snyder L. E., de Pater I., Forster J. R., Palmer P., Kuan Y.-J., Williams W. R., Cheung C. C., and Smith B. R. (2002) Morphology of HCN and CN in Comet Hale-Bopp (1995 O1). *Icarus, 157,* 193–204.

Wyckoff S. and Wehinger P. A. (1976) Molecular ions in comet tails. *Astrophys. J., 204,* 604–615.

Yeomans D. K., Chodas P. W., Szutowicz S., Sitarski G., and Krolikowska M. (2004) A review of cometary orbit determination and nongravitational forces. In *Comets II* (M. C. Festou et al., eds.), this volume. Univ. of Arizona, Tucson.

Zucconi J. M. and Festou M. C. (1985) The fluorescence spectrum of CN in comets. *Astron. Astrophys., 150,* 180–191.